bioRxiv preprint doi: https://doi.org/10.1101/465930; this version posted November 8, 2018. The copyright holder for this preprint (which was not certified by peer review) is the author/funder. All rights reserved. No reuse allowed without permission.

Enhanced cell-cell contact stability upon Fibroblast Growth factor Receptor-N-cadherin cross-talk

Thao Nguyen[1], Laurence Duchesne[2], Nicole Bogetto[1], David D. Fernig[3], Chandra Murade[1], Benoit Ladoux[1], René-Marc Mège[1]

[1] Institut Jacques Monod, CNRS, Université Paris Diderot, 15 Rue Hélène Brion 75205 Paris Cedex 13, France.

[2] Univ Rennes, CNRS, IGDR (Institute of Genetics and Development of Rennes) – UMR 6290, F-35000 Rennes, France.

[3] University of Liverpool, Institute of Integrated Biology, Department of Biochemistry; Centre for Cell Imaging, Liverpool, L69 7ZB, UK.

*Corresponding author: René Marc Mège, Institut Jacques Monod, 15 Rue Hélène Brion, 75205 Paris Cedex, France, tel : 33 1 57 2780 67, mail : rene-marc.mege@ijm.fr

Running Head: **Strengthening N-cadherin cell-cell contacts by FGFR.**

bioRxiv preprint doi: https://doi.org/10.1101/465930; this version posted November 8, 2018. The copyright holder for this preprint (which was not certified by peer review) is the author/funder. All rights reserved. No reuse allowed without permission.

Abbreviations:

FGF: Fibroblast Growth Factor

FGFR: Fibroblast Growth Factor Receptor

FP: Fluorescent Protein

FN: Fibronectin

FRAP: Floorescence Recovery After Photobleaching

GFP: Green Fluorescent Protein

Ncad: N-cadherin

PBS: Phosphate Buffer Saline

RTK: Receptor Tyrosine Kinase

SEM: Standard Error of the Mean

bioRxiv preprint doi: https://doi.org/10.1101/465930; this version posted November 8, 2018. The copyright holder for this preprint (which was not certified by peer review) is the author/funder. All rights reserved. No reuse allowed without permission.

Abstract

N-cadherin adhesion has been reported to enhance cancer and neuronal cell migration by mediating either actomyosin-based force transduction or initiating Fibroblast Growth Factor Receptor (FGFR)-dependent biochemical signaling. We show here that FGFR1 reduces N-cadherin-mediated cell migration. Both proteins are co-stabilized at cell-cell contacts through direct interaction. As a consequence, cell adhesion is strengthened limiting the migration of cells on N-cadherin. Both the inhibition of migration and the stabilization of cell adhesions require the FGFR activity stimulated by N-cadherin engagement. FGFR1 stabilizes N-cadherin at the cell membrane by decreasing its endocytosis through a pathway involving Src and p120. Moreover, FGFR1 stimulates the anchoring of N-cadherin to actin. We found that the migratory behavior of cells depends on an optimum balance between FGFR-regulated N-cadherin adhesion and actin dynamics. Based on these findings we propose a positive feed-back loop between N-cadherin and FGFR at adhesion sites limiting N-cadherin-based single cell migration.

bioRxiv preprint doi: https://doi.org/10.1101/465930; this version posted November 8, 2018. The copyright holder for this preprint (which was not certified by peer review) is the author/funder. All rights reserved. No reuse allowed without permission.

Introduction

Cell adhesion and migration are two central processes in morphogenesis and wound healing. Their dysregulation is associated with diseases such as congenital malformations, neurological disorders and cancers. Cells during embryogenesis and metastasis adhere and migrate on, or through, extracellular matrices thanks to their integrin receptors (Huttenlocher and Horwitz, 2011). However, many cells such as border cells in the *Drosophila* egg chamber (Prasad et al., 2011), neuronal precursors (Jossin and Cooper, 2011; Luccardini et al., 2013) or cancer cells also directly adhere and migrate on other cell's membranes. In these cases, cell migration is also regulated by cadherin-mediated cell adhesion which physically holds cells together (Mayor and Etienne-Manneville, 2016). As a result, changes in expression and/or function of cadherins have major impacts on cell migration during neural development (Redies and Takeichi, 1996; Scarpa et al., 2015; Treubert-Zimmermann et al., 2002) and tumour cell invasion (Kashima et al., 2003; van Roy, 2014; Wheelock et al., 2001).

Cadherins are the intercellular homophilic ligands of *Adherens Junctions* (AJ) involved in the cohesion and homeostatic maintenance of solid tissues (Meng and Takeichi, 2009). Cadherins provide anchorage between neighboring cells thanks to their interaction with the contractile actomyosin network through the adaptor proteins catenins α, β and p120 (Mege and Ishiyama, 2017). E-cadherin, the major cadherin expressed in epithelia is required for epithelial cell cohesion (Gumbiner et al., 1988) and is recognized as a tumor suppressor (Kashima et al., 2003; van Roy and Berx, 2008). N-cadherin, the neuronal cadherin, although required for the cohesive interaction and organization of neuroepithelial cells (Kadowaki et al., 2007), mediates however weaker cell-cell adhesion and has been associated with cell migration in a large range of tissues, in both physiological and pathological processes (Derycke and Bracke, 2004; Nguyen and Mege, 2016; Suzuki and Takeichi, 2008). During neural development, N-cadherin ensures the labile adhesion between post-mitotic neurons and radial glial cells allowing radial neuronal precursor migration (Franco et al., 2011; Jossin and Cooper, 2011). During this process, N-cadherin undergoes active endocytosis maintaining proper cell surface levels and allowing the effective locomotion of neurons (Jossin and Cooper, 2011). N-cadherin is also required for proper long distance migration and maintained polarization of tangentially migrating interneuron precursors (Luccardini et al., 2013). *In vitro*, N-cadherin has been long recognized as a stimulating substrate for neurite outgrowth (Bard et al., 2008; Bixby and Zhang, 1990; Letourneau et al., 1990; Matsunaga et al., 1988;

bioRxiv preprint doi: https://doi.org/10.1101/465930; this version posted November 8, 2018. The copyright holder for this preprint (which was not certified by peer review) is the author/funder. All rights reserved. No reuse allowed without permission.

Williams et al., 1994). Two pathways have been involved in N-cadherin-induced neurite outgrowth: the mechanical coupling of adhesion sites to the actomyosin tread milling generating the traction forces necessary to propel the growth cones (Bard et al., 2008; Giannone et al., 2009) and the activation of an FGFR-dependent biochemical signalling cascades (Boscher and Mege, 2008; Williams et al., 1994).

FGFRs (Fibroblast Growth Factor Receptors) belong to the family of single pass transmembrane Receptors Tyrosine Kinases (RTK). FGFRs, activated by the binding of their cognate ligands FGFs, trigger numerous intracellular signalling cascades orchestrating key cellular events during development and pathogenesis, including cell adhesion and migration (Lemmon and Schlessinger, 2010; McIntosh et al., 2000). In humans, a wide spectrum of abnormalities is associated to mutations in FGFRs including skeletal dysplasia, deafness, dermatologic disorders and ocular abnormalities (McIntosh et al., 2000). In mice, the loss of expression of FGFR1 disrupts the migration of epidermal cells from the primitive streak; a phenotype that can be rescued by down-regulating E-cadherin-mediated intercellular adhesion (Ciruna and Rossant, 2001; Ciruna et al., 1997; Deng et al., 1994; Yamaguchi et al., 1994). In *Drosophila*, the migration of tracheal cells requires FGFR signaling regulating dynamic cytoskeletal reorganizations (Chu et al., 2013; Lebreton and Casanova, 2016; Peterson and Krasnow, 2015).

Dysfunctions of N-cadherin and FGFRs both induce pathological migrations that are most visible in the case of cancer. Dysplastic cells acquire motility and invasiveness by upregulating N-cadherin in melanoma (Li et al., 2001), bladder (Rieger-Christ et al., 2004), prostate (Kolijn et al., 2015), lung (Nakashima et al., 2003) or breast cancers (Nagi et al., 2005). Mutations in FGFRs are associated to pancreatic, endometrial, bladder, prostate, lung and breast cancers (Porta et al., 2017; Wesche et al., 2011). Little is known however about the combined effects of N-cadherin and FGFR activities on embryonic and cancer cell adhesion and migration. Existing literature reports on a synergistic action between N-cadherin and FGFRs in the regulation of the pluripotency of epiblast stem cells (mEpiSC) (Takehara et al., 2015), the survival of ovarian cells (Trolice et al., 1997) and the differentiation of osteogenic cells (Debiais et al., 2001). The overexpression of N-cadherin in mEpiSC cells prevents the downregulation of FGFR at the plasma membrane after FGF2 addition (Takehara et al., 2015). FGF and N-cadherin maintain granulosa and ovarian cells viability *in vitro* by stimulating phosphorylation of FGFR (Trolice et al., 1997). The expression of a constitutively active form of FGFR increases the expression of N-cadherin reinforcing cell-cell adhesion in human osteogenic cells (Debiais et al., 2001).

bioRxiv preprint doi: https://doi.org/10.1101/465930; this version posted November 8, 2018. The copyright holder for this preprint (which was not certified by peer review) is the author/funder. All rights reserved. No reuse allowed without permission.

A functional relationship between FGFR and N-cadherin has been reported during neurite outgrowth (Boscher and Mege, 2008; Williams et al., 1994). FGFR and N-cadherin were reported to co-cluster and interact at the plasma membrane of neuronal cells (Boscher and Mege, 2008; Utton et al., 2001). The expression of a dominant negative FGFR has been reported to inhibit neurite growth as well as FGFR phosphorylation stimulated by N-cadherin (Brittis et al., 1996). In breast cancer cells, transfection of exogenous N-cadherin increases cell migration (Hazan et al., 1997). FGFR and N-cadherin are found in the same immunocomplex and N-cadherin prevents FGFR from undergoing ligand-induced-internalization, resulting in FGFR stabilisation at the plasma membrane, and ultimately in sustained FGFR signalling (Suyama et al., 2002). In human pancreatic cancer xenografts, inhibition of FGFR leads to the decreased expression of N-cadherin and to the reduction in cancer cell invasion (Taeger et al., 2011). Altogether, these data suggest that N-cadherin and FGFR synergize to generate signals which alter migratory or/and invasive behaviours of normal as well as cancer cells.

To dissect the reciprocal interplay between FGFR1 and N-cadherin, we expressed both FP (Fluorescent Protein)-tagged receptors in HEK cells and analyzed the consequences on cell-cell adhesion and N-cadherin-dependent cell migration. Using a single cell migration model on N-cadherin coated lines, we show here that FGFR1 overexpression reduces the migration of N-cadherin expressing cells. Both proteins are co-recruited and co-stabilized at cadherin-mediated cell contacts as revealed by quantitative fluorescence and FRAP analysis, through direct interaction of their extracellular domains. As a consequence, N-cadherin-mediated cell contacts are strengthened limiting the migration of cells on N-cadherin coated surfaces. Both the inhibition of N-cadherin-mediated migration and the stabilization of N-cadherin at cell contacts require the FGFR activity, which is itself stimulated by N-cadherin engagement. Cell surface biotinylation and flow cytometry analysis further showed that FGFR stabilizes N-cadherin at the cell membrane by decreasing its internalization. FGFR1 expression triggers an increase in N-cadherin-bound immunocomplexes of activated Src and the decreases in phosphorylation of its target p120 catenin, a well-known regulator of cadherin trafficking. We then showed that p120 and Src are both involved in the stabilization of N-cadherin at cell-cell contacts and in the negative regulation of N-cadherin-mediated migration, induced by FGFR1. Moreover, we found that FGFR1 stimulates the anchoring of N-cadherin to actin and that the migratory behavior of cells depends on an optimum balance between N-cadherin-mediated adhesion and actin dynamics. Altogether these data support the

bioRxiv preprint doi: https://doi.org/10.1101/465930; this version posted November 8, 2018. The copyright holder for this preprint (which was not certified by peer review) is the author/funder. All rights reserved. No reuse allowed without permission.

hypothesis that FGFR1 activity strengthens N-cadherin mediated cell-cell adhesion, and as a result decreases N-cadherin-dependent single cell migration.

bioRxiv preprint doi: https://doi.org/10.1101/465930; this version posted November 8, 2018. The copyright holder for this preprint (which was not certified by peer review) is the author/funder. All rights reserved. No reuse allowed without permission.

Results

FGFR1 expression inhibits N-cadherin-mediated cell migration

To study N-cadherin-mediated cell migration we developed a model in which isolated Fluorescent Protein (FP)-tagged N-cadherin expressing HEK cells (Ncad cells) were allowed to migrate on Ncad-Fc-coated stripes. To study the impact of Fibroblast Growth Factor Receptor 1 (FGFR1) on the regulation of N-cadherin-dependent single cell migration we generated double transfected Ncad/FGFR cells expressing also FP-tagged FGFR1. Ncad and Ncad/FGFR cells were seeded on 10 µm width Ncad-Fc-coated lines and then followed by videomicroscopy over 20 hours **(Fig. 1A, Video 1)**. While Ncad cells migrate efficiently, Ncad/FGFR cells were almost stationary. The trajectories of single cells were manual tracked and the cell displacement plotted over time (**Fig. 1B**). Ncad cells were very mobile covering a total displacement up to 400 µm over 20 hours, at a mean speed of 29.9 ± 4.7 µm/hour (**Fig. 1D**), with a very few inversions of direction of migration**(Fig. 1E)**. The migration of Ncad/FGFR cells was drastically inhibited with a mean speed of 5.6 ± 2.8 µm/hour (**Fig. 1B,D**). We further analyzed the migration of Ncad/FGFR cells treated with the FGFR kinase activity inhibitor PD173074 **(Fig.1A-E)**. Treatment with the inhibitor restored a migratory behavior of Ncad/FGFR cells close to the one of Ncad cells with a migration speed of 22.9 ± 1.3 µm/hour, indicating that the inhibition of migration on N-cadherin observed in cells expressing FGFR1 requires the activity of the receptor. Although the migration speed was restored, FGFR inhibitor treated Ncad/FGFR cells displayed a higher frequency of inversion of migration orientation compared to Ncad cells **(Fig. 1B, E)**. While this parameter may not be very robust for cells having such reduced displacements, our observations suggest that FGFR activity may increase the ability of cells to maintain their polarity. Altogether these data indicate that FGFR1 strongly impairs the migration of cells on N-cadherin in a process depending on its kinase activity.

Interestingly, Ncad/FGFR cells tend to be more spread than Ncad cells, a trend that was reverted in the presence of the FGFR inhibitor (**Fig. 1C, Video 1**). Measurement of the projected cell areas showed a mean cell spreading was of 302.8 ± 13.38 μm^2 for Ncad cells, raised to 764.7 ± 24.91 μm^2 for Ncad/FGFR cells, while it felt down to 562.6 ± 10.63 μm^2 in the presence of FGFR inhibitor. Thus the decrease in single cell migration on Ncad-Fc substrate goes with an increased N-cadherin-mediated adhesion. Plotting the mean cell speed

bioRxiv preprint doi: https://doi.org/10.1101/465930; this version posted November 8, 2018. The copyright holder for this preprint (which was not certified by peer review) is the author/funder. All rights reserved. No reuse allowed without permission.

as a function of the projected cell area, we confirmed an inverse correlation between these two parameters: the more the cells spread on N-cadherin, the slower they migrate **(Fig. 1F)**. Ncad/FGFR cells displaying an extensive spreading and a reduced migration speed. Ncad cells clustered in a region of small cell area / high migration speed whereas Ncad/FGFR cells clustered in a region of the graph with high cell area/low migratory speed, and Ncad/FGFR cells treated with FGFR inhibitor clustered close to Ncad cells. Thus, the reduced migration of FGFR1 expressing cells could result from a strengthening of cadherin-mediated adhesion on the Ncad-Fc coated lines.

N-cadherin and FGFR1 are co-stabilized at cell-cell contacts

We thus hypothesized that FGFR1 increased N-cadherin-mediated cell-cell adhesion by affecting the dynamics of N-cadherin molecules at these sites. To test this hypothesis and at the same time follow the dynamics of FGFR1, we performed dual wavelength FRAP (Fluorescence Recovery After Photobleaching) experiments at cell-cell contacts of HEK cells expressing DsRed-Ncad or GFP-FGFR1 alone, or both molecules at the same time **(Fig. 2A, B)**. When N-cadherin was expressed alone, we detected a mobile fraction at the cell-cell contacts of 61.3 ± 2.7 %, in agreement with previous reports (Lambert et al., 2007). Expression of FGFR1 significantly decreased the mobile fraction of N-cadherin (38.2 ± 3.4 %) while treatment with the FGFR kinase inhibitor restored N-cadherin mobile fraction level (62.3 ± 2.3 %) close to the one found in Ncad cells. Expression of N-cadherin significantly decreased the mobile fraction of FGFR1 at cell-cell junctions, which was of 58.9 ± 2.3 % in the absence of N-cadherin and dropped to 44.0 ± 3.7 % when N-cadherin was co-expressed **(Fig. 2C)**. To test whether this cross regulation regarding FGFR1 and N-cadherin mobility was specific to N-cadherin, similar experiments using mCherry-tagged E-cadherin (mCherry-Ecad) instead of DsRed-Ncad were performed. Results showed that E-cadherin expression did not affect the dynamics of FGFR1 molecule at cell-cell contacts **(Fig. 2C)**. Similarly, FGFR1 expression did not modify the mobile fraction of E-cadherin at cell-cell contacts **(Fig. 2D)**. Thus, FGFR1 and N-cadherin specifically co-stabilize each other at N-cadherin-mediated contacts. This co-stabilization may lead to the strengthening of N-cadherin mediated adhesion which may explain the increased spreading of cells on Ncad-coated lines upon FGFR1 expression.

bioRxiv preprint doi: https://doi.org/10.1101/465930; this version posted November 8, 2018. The copyright holder for this preprint (which was not certified by peer review) is the author/funder. All rights reserved. No reuse allowed without permission.

FGFR1 stimulates junctional N-cadherin accumulation and strengthen cell-cell contacts

To confirm the strengthening effect of FGFR expression on N-cadherin-mediated adhesion, we quantified the accumulation of DsRed-N-cadherin at cell-cell contacts in monolayers of HEK cells expressing or not FGFR1-GFP. Cell-cell contacts accumulated more N-cadherin and were straighter for Ncad/FGFR than for Ncad cells as confirmed by DsRed-Ncad intensities analysis **(Fig. 3A)**. FGFR inhibitor treatment annihilated the effect of FGFR1 expression both on the straightness and junctional accumulation of N-cadherin, indicating that the kinase activity of the receptor is required for the strengthening of N-cadherin-mediated cell contacts. Accordingly, analyzing N-cad distribution at cell-cell contacts revealed an increased accumulation of junctional N-cadherin in the presence of FGFR1 in cell doublets grown on fibronectin-coated lines **(Fig. 3B)**, as well as in resuspended cell doublets **(Fig. 3C, Fig. S1).** Moreover, the analysis of signal heterogeneity at cell-cell contacts revealed that the recruitment of N-cadherin in clusters was more prominent in Ncad/FGFR than in Ncad cells **(Fig. 3C, Fig. S1)**.

To determine the impact of this junctional N-cadherin stabilization on cell-cell contact stability, we followed by live imaging the disassembly of cell-cell contacts upon chelation of Ca^{2+} ions in cell monolayers **(Fig. 4A)**. Ncad cells had detached from each other 2 minutes after EGTA addition, while Ncad/FGFR cells remained cohesive. Moreover, inhibition of FGFR kinase activity significantly increased cell dispersion of Ncad/FGFR cells. This result was further confirmed by quantitative analysis of cell-cell contact life-time following Ca^{2+} depletion **(Fig. 4B, C)**. FGFR1 expression tripled the cell-cell contact life-time, a stabilization that was fully reverted by inhibiting FGFR kinase activity. Thus the kinase activity of the receptor is required for the strengthening of N-cadherin mediated cell-cell contacts. To test more directly the effect of FGFR1 on the strength of N-cadherin-mediated adhesions, we probed the response to force of contacts between Ncad-Fc-coated magnetic beads and Ncad or Ncad/FGFR cells. Beads were let to interact with the cell surface for 30 minutes, before being probed for displacement under force by approaching the magnetic rod **(Fig. 4D, E, Video 2)**. The semi-quantitative analysis of bead behavior showed that significantly fewer beads were displaced or detached from the cell surface of Ncad/FGFR cells indicating that the binding strength was higher on Ncad/FGFR cells compared to Ncad cells **(Fig. 4F)**. Moreover, the inhibition of the FGFR kinase activity restored bead detachment/displacement in proportions similar to those observed for Ncad cells. For the population of beads that were detached under force, the distance between bead and the magnetic rod at which the bead was teared off the

bioRxiv preprint doi: https://doi.org/10.1101/465930; this version posted November 8, 2018. The copyright holder for this preprint (which was not certified by peer review) is the author/funder. All rights reserved. No reuse allowed without permission.

cell membrane (breaking distance) was recorded **(Fig. 4E)**. The mean breaking distance was of 28.5 ± 0.9 µm for Ncad cells and 14.3 ± 0.6 µm for Ncad/FGFR cells, respectively. Inhibition of FGFR in Ncad/FGFR cells increases the breaking distance to 21.4 ± 0.9 µm. After calibration, one can estimate the actual forces at which the N-cadherin-mediated adhesions between the bead and the plasma membrane were disrupted **(Fig. 4D)**. FGFR1 expression consistently increased the disruption force of Ncad mediated cell contacts from 5.9 ± 0.1 nN to 7.3 ± 0.1 nN. Inhibition of the receptor activity significant attenuated this effect (6.5 ± 0.1nN), which proves that FGFR activity is required to increase the mechanical resistance of N-cadherin-mediated adhesion.

N-cadherin and FGFR1 interact to sustained activation of FGFR1

We described so far an effect of FGFR1 overexpression on N-cadherin contact strengthening which requires the kinase activity of the receptor although no exogenous FGF ligand was added. Furthermore, FGFR1 and N-cadherin are co-stabilized at the cadherin-mediated cell contacts. Therefore, we hypothesized that the increased residence of FGFR at cell-cell contacts induced by N-cadherin-mediated adhesion may induce a FGF-independent activation of the receptor which may rely on direct interactions of these two proteins as previously reported in neuronal cells (Boscher and Mege, 2008). To confirm this hypothesis, the level of binding of Ncad-Fc to immobilized FGFR1 extracellular domain (FGFR1-ST) was measured using an optical biosensor. Results showed a direct interaction between N-cadherin and FGFR1 extracellular domains with an affinity, calculated from the kinetic parameters of the interaction, of 106 nM (K_D = 106 ± 25 nM) (**Fig. 5A and Table 1**). This interaction was confirmed by co-immunoprecipitation **(Fig. 5B)**. N-cadherin was specifically co-immunoprecipitated with GFP-FGFR1 out of protein extracts of HEK cells co-expressing the two proteins. Interestingly, the co-precipitation was strongly reduced when FGFR kinase activity was inhibited.

To probe whether N-cadherin induces FGFR activation, we followed the phosphorylation of the tagged receptor in Ncad and Ncad/FGFR cells **(Fig. 5C)**. FGFR1 phosphorylation was significantly increased in Ncad/FGFR cells compared to FGFR1 only expressing cells. To further provide evidence that FGFR1 was activated by N-cadherin-mediated adhesion, we followed the activation of Erk1/2, a well-known downstream relay of FGFR activation, following Ca^{2+} switch in C2C12 cells that express endogenous N-cadherin

bioRxiv preprint doi: https://doi.org/10.1101/465930; this version posted November 8, 2018. The copyright holder for this preprint (which was not certified by peer review) is the author/funder. All rights reserved. No reuse allowed without permission.

(Gavard et al., 2004) and FGFRs (Kontaridis et al., 2002) **Fig. S2)**. As a control we observed that Erk1/2 phosphorylation was significantly increased in FGF2 treated C2C12 cells **(Fig. S2A)**. We then followed FGFR activation in cells maintained in low Ca^{2+} then switched to 2 mM Ca^{2+} to trigger N-cadherin engagement. Addition of Ca^{2+} for 10 minutes to Ca^{2+}-depleted cells significantly increased Erk1/2 phosphorylation in the absence but not in the presence of the FGFR inhibitor **(Fig. S2B)**, strongly suggesting that N-cadherin engagement triggers the activation of the FGFR1. At this point, our results suggest a two-way communication between FGFR1 and N-cadherin resulting from their direct interaction. The stabilization of FGFR1 by N-cadherin at cell-cell contacts allows its activation. The activation of FGFR1 increases junctional N-cadherin junctional recruitment and stabilization, which in turn strengthens N-cadherin-mediated cell adhesion and reduces N-cadherin-dependent cell migration.

FGFR1 stabilizes N-cadherin at the plasma membrane through downregulation of its endocytosis.

To determine whether FGFR1 expression increases N-cadherin prevalence at the plasma membrane, we first performed cell surface biotinylation on live Ncad and Ncad/FGFR HEK cells followed by protein extraction, streptavidin immunoprecipitation then anti-N-cadherin immunoblotting. The fraction of cell surface exposed biotin-labelled N-cadherin was significantly higher in Ncad/FGFR than in Ncad cells. It was strongly decreased in Ncad/FGFR cells grown in the presence of the FGFR inhibitor **(Fig. 6A)**. Thus, FGFR1 significantly increases the fraction of N-cadherin accumulated at the plasma membrane in a process depending on its kinase activity. A first hint on the way FGFR1 may regulate N-cadherin availability at the cell surface was given by imaging DsRed-Ncad and analyzing its distribution at the outer surface and in the cytoplasm of either Ncad or Ncad/FGFR expressing cells thanks to flow cytometry imaging **(Fig. 6B)**. The internalization score in the internal part of the cells was of 1.32 and 1.09 for the Ncad cells and Ncad/FGFR cells, respectively, suggesting that FGFR1 expression may increase N-cadherin exocytosis or decrease N-cadherin endocytosis.

Accordingly, when imaging DsRed-Ncad in cells migrating on fibronectin-coated lines **(Video 3)**, we observed N-cadherin vesicles trafficking from the leading edge to the rear of the cells. These vesicles were significantly more prominent in Ncad than in Ncad/FGFR cells, suggesting that the trafficking of N-cadherin was reduced in the latter **(Fig. 6C)**. We thus

bioRxiv preprint doi: https://doi.org/10.1101/465930; this version posted November 8, 2018. The copyright holder for this preprint (which was not certified by peer review) is the author/funder. All rights reserved. No reuse allowed without permission.

questioned the role of endocytosis as a possible mechanism of the regulation of cell surface N-cadherin by FGFR1. To quantify N-cadherin endocytosis, cell surface proteins were biotinylated in cold then cells were switched at 37°C to allow endocytosis to resume for 40 minutes before cleavage of cell surface-exposed biotin. Proteins were then extracted, and precipitated with either streptavidin or anti-N-cadherin antibodies than analyzed by Western blot. The ratio of biotin-labelled N-cadherin on total immunoprecipitated N-cadherin (quantifying the endocytic pool), was significant reduced in Ncad/FGFR cells compared to Ncad cells **(Fig. 6D)**. In order to confirm that FGFR1 expression indeed affected N-cadherin endocytosis, we treated Ncad and Ncad/FGFR cells with hydroxyl-dynasore, an inhibitor of endocytosis. The endocytosed fraction of N-cadherin was decreased by this treatment in Ncad cells to reach the levels measured for Ncad/FGFR cells, while it was not affected by this treatment in Ncad/FGFR cells, supporting the notion that FGFR1 indeed regulates N-cadherin levels at the plasma membrane by inhibiting its endocytosis. This inhibition of N-cadherin endocytosis in the presence of FGFR1 was significantly reduced in the presence of FGFR inhibitor **(Fig. S3)**, Thus, FGFR1 through its kinase activity reduces the endocytosis of N-cadherin, resulting in higher levels of N-cadherin present at the plasma membrane which could contribute to the reinforcement of N-cadherin-mediated cell contacts.

p120 is involved in FGFR1-dependent stabilization of N-cadherin mediated cell-cell contacts and inhibition of migration

The protein p120 is known as a positive posttranslational regulator of cadherin expression at the plasma membrane (Ireton et al., 2002). It was reported to stabilize cadherins at cell-cell contacts by regulating their trafficking either to the plasma membrane (Chen et al., 2003) or from the plasma membrane to endocytic compartments (Davis et al., 2003). Thus, we asked whether the interaction of N-cadherin with p120 could be involved in the regulation of N-cadherin endocytosis by FGFR1. The analysis of the distribution GFP-p120 in cell doublets seeded on fibronectin-coated lines revealed that FGFR1 expression increased p120 recruitment at cell-cell contacts **(Fig. 7A)** in agreement with the enhanced N-cadherin accumulation **(Fig. 3B)**. To test the implication of p120 in N-cadherin stabilization at cell-cell contacts, we generated transfectants expressing FP tagged FGFR1 and the NcadAAA mutant. The AAA mutation at position 764 in E-cadherin (Thoreson et al., 2000) was described to impair its binding to p120 and a similar mutation has been described in N-cadherin

bioRxiv preprint doi: https://doi.org/10.1101/465930; this version posted November 8, 2018. The copyright holder for this preprint (which was not certified by peer review) is the author/funder. All rights reserved. No reuse allowed without permission.

(Thoumine et al., 2006). We then realized FRAP experiments on Ncad/FGFR and NcadAAA/FGFR cells **(Fig. 7B)**. The mobile fraction of the mutated N-cadherin was significantly higher (50.6 ± 1.6 %) than the one of wild type N-cadherin (28.8 ± 1.1 %). It was similar to the one of wild type N-cadherin in cells expressing N-cadherin alone (61.3 ± 2.7 %, **Fig.2B)**, suggesting that the binding of p120 to N-cadherin is involved in the stabilization of N-cadherin at cell-cell contacts induced by FGFR1 expression. To see whether the ability of N-cadherin to bind p120 affects also the regulation of N-cadherin-mediated cell migration by FGFR1, we compared the migration of Ncad/FGFR and NcadAAA/FGFR single cells on Ncad-Fc coated lines **(Fig. 7C, D and Video 4)**. NcadAAA/FGFR cells migrated faster than Ncad/FGFR cells, with a mean speed of 26.8 ± 2.6 µm/h, compared to 7.8 ± 5.1 µm/h for the latter. NcadAAA/FGFR cells displayed similar migration speed than Ncad cells **(Fig 1D)**. One can appreciate as well the inverse relation between migration speed and spreading area; NcadAAA/FGFR cells displayed reduced spreading areas and fast migration speeds **(Fig. 7D)** whereas Ncad/FGFR cells were characterized by higher spreading areas and lower migration speeds **(Fig. 1D)**. Thus, preventing the binding of N-cadherin to p120 strongly decreases junctional N-cadherin stabilization induced by FGFR1 and prevents as well the FGFR1-dependent inhibition of single cell migration on N-cadherin.

p120 expression levels may determine steady-state levels of functional cadherins by regulating their turnover at the cell surface (Davis et al., 2003). We thus analyzed the expression levels of p120 in Ncad, FGFR and Ncad/FGFR cells **(Fig. S4A)**. The total cellular levels of p120 were not significantly affected indicating that the expression of FGFR1 does not affect the expression level of p120. The presence of the N-terminal phosphorylation domain of p120, containing various phosphorylation sites including tyrosine residues phosphorylated by Src family kinases, has been reported to regulate negatively N-cadherin stability at the plasma membrane (Ireton et al., 2002; Kourtidis et al., 2015; Mariner et al., 2001). We thus analyzed the phosphorylation on Y228 of total p120 and of the p120 pool engaged in a complex with N-cadherin **(Fig. S4B,C)**. FGFR1 expression did not affect the ratio of p120 Y228 phosphorylation in total extracts. It decreased however the phosphorylation on Y228 of N-cadherin-associated p120, while further treatment of Ncad/FGFR cells with the FGFR kinase inhibitor had an opposite effect. Thus, the FGFR activity may stabilize N-cadherin at the plasma membrane by negatively regulating p120 Y228 phosphorylation.

bioRxiv preprint doi: https://doi.org/10.1101/465930; this version posted November 8, 2018. The copyright holder for this preprint (which was not certified by peer review) is the author/funder. All rights reserved. No reuse allowed without permission.

The effects of FGFR1 on N-cadherin-mediated adhesion and migration involve Src family kinases

p120 has been reported initially as a substrate of Src family kinases (Kanner et al., 1991; Mariner et al., 2001), itself a downstream target of FGFR1 (Ren et al., 2011; Zhan et al., 1994). We thus analyzed the effect of a Src kinase family inhibitor PP2 on p120 phosphorylation level **(Fig. S4B)**. Src inhibition had no effect on the level of phosphorylation of total p120. However, it restored high level of phosphorylation of N-cadherin-bound p120 in Ncad/FGFR cells, albeit not at levels observed after FGFR inhibition. These results suggest that FGFR1 activity may repress the phosphorylation of N-cadherin-bound p120 in part through a Src family kinases-dependent pathway. Thus, we investigated the levels of Src activation, through the phosphorylation of its tyrosine 416, in N-cadherin immunocomplexes in Ncad, Ncad/FGFR and Ncad/FGFR+inh cells **(Fig. 8A)**. FGFR1 expression led to an increase in Src catalytic domain phosphorylation. FGFR inhibition prevented this increase in activated Src, indicating that FGFR1 kinase activity is responsible of the increase in activated Src associated to N-cadherin.

In order to determine the involvement of Src in the stabilization of N-cadherin-mediated adhesion induced by FGFR1 expression, we analyzed the effect of Src inhibition on the mobility of N-cadherin at cell-cell contacts. FRAP experiments revealed that the inhibition of Src kinase activity restored high levels of junctional N-cadherin mobile fraction in Ncad/FGFR, comparable to those determines in cells that do not express the receptor **(Fig. 8B)**. To determine the role of Src in the modulation of N-cadherin-mediated cell migration by FGFR1, we submitted Ncad/FGFR cells to the single cell migration assays on Ncad-Fc-coated lines in the absence or in the presence of the Src inhibitor PP2 **(Fig. 8C and Video 5)**. Ncad/FGFR cells treated with the Src inhibitor displayed a strong stimulation of their migration properties with a mean speed of migration comparable to the one of Ncad cells. Thus, Src inhibition counteracts both the stabilization of N-cadherin cell-cell contact and the inhibition of N-cadherin-mediated migration induced by FGFR1 expression. Altogether, these data suggest that FGFR1 expression triggers the activation of Src in N-cadherin complexes that may regulate the stability of junctional cadherin and the migratory response of N-cadherin expressing cells. However, since FGFR induces at the same time the activation of Src and a decrease in p120 tyrosine phosphorylation in N-cadherin immunocomplexes, they are unlikely acting directly upstream on of the other in the same signaling cascade.

bioRxiv preprint doi: https://doi.org/10.1101/465930; this version posted November 8, 2018. The copyright holder for this preprint (which was not certified by peer review) is the author/funder. All rights reserved. No reuse allowed without permission.

FGFR1 stiffens the anchoring of N-cadherin to actin network

The mechanocoupling between cadherin complexes and the underlying actomyosin network has been reported as a major mechano-signalling mechanism leading to the reinforcement of cell-cell contacts and regulating neuronal cell migration (Giannone et al., 2009; Mege and Ishiyama, 2017). To further evidence the effect of FGFR activity on the functionality of the mechanical link between N-cadherin and actin reported in Figure 4 E-G, we analyzed the retrograde flow of F-actin in the lamellipodia of cells spread on N-cadherin, previously reported as a proxy the coupling of cadherin to the treadmilling actin (Plestant et al., 2014; Strale et al., 2015). We quantified the actin retrograde flow in the lamellipodia of LifeAct-GFP expressing C2C12 myogenic cells spread on Ncad- coated surfaces, treated or not with the FGFR inhibitor **(Fig. 9A**; **Video 6**). The speed of F-actin rearward flow was increased by 40% in cells treated with the FGFR inhibitor compared with cells treated by the vehicle alone, indicating that the functional coupling of N-cadherin adhesion complexes to F-actin was decreased following FGFR activity inhibition. This result suggests that in these myogenic cells, the FGFR activity constitutively stimulates the functional coupling of N-cadherin to the actin cytoskeleton, in agreement with data obtained in transfected HEK cells.

To further test whether the modulation of this mechanocoupling was instrumental in regulating N-cadherin-mediated cell migration, transfected Ncad and Ncad/FGFR HEK cells were treated with the Arp2/3 inhibitor CK 666 and analyzed for their migration on Ncad-coated lines **(Fig. 9B; Video 7)**. Interestingly, while the inhibition of branched actin polymerization almost fully abrogated the migration of Ncad cells, it significantly increased the migration of Ncad/FGFR cells on N-cadherin (compare **to Fig. 1**). These observations indicate a bimodal implication of branched actin polymerization in N-cadherin-mediated adhesion that is necessary for the migration displaying mild adhesion (Ncad cells), but prevents the migration of tightly adhering Ncad-FGFR cells likely through the destabilization of adhesions. Altogether, cell migration on N-cadherin may require an optimal balance between N-cadherin-mediated adhesion and deadhesion that depends on the strength of the N-cadherin-F-actin mechanocoupling. To further support this notion, we analyzed the implication of non-muscle myosin II, also contributing to the actin treadmilling in the lamellipodia. Treatment with the myosin II inhibitor similarly blocked the migration of Ncad cells on N-cadherin lines and stimulated the one of Ncad/FGFR cells **(Fig. S5)**. Altogether,

bioRxiv preprint doi: https://doi.org/10.1101/465930; this version posted November 8, 2018. The copyright holder for this preprint (which was not certified by peer review) is the author/funder. All rights reserved. No reuse allowed without permission.

these data indicate that FGFR1 activity increases the coupling of N-cadherin complexes to the underlying cytoskeleton. The resulting strengthening of N-cadherin-mediated contacts contributes to the inhibition of cell migration on the N-cadherin substrate.

bioRxiv preprint doi: https://doi.org/10.1101/465930; this version posted November 8, 2018. The copyright holder for this preprint (which was not certified by peer review) is the author/funder. All rights reserved. No reuse allowed without permission.

Discussion

Although cadherin and FGFRs dysregulation and/or dysfunction are observed in many type of cancers, their relation to cell migration and invasion remains unclear. N-cadherin facilitates cell migration in numerous developmental and pathological processes whereas FGFRs are either enhancers or repressors of cell migration depending on the context. In light of reported crosstalk between E-cadherin and EGFR (McCrea et al., 2015) and VE-cadherin and VEGFR (Carmeliet and Collen, 2000; Giannotta et al., 2013) suggesting that cell type specific cadherin/tyrosine kinase growth factor receptor cross-talks have strong impact during developmental and pathological processes, a crosstalk between N-cadherin and FGFR has been proposed (Boscher and Mege, 2008; Nguyen and Mege, 2016; Suyama et al., 2002; Williams et al., 1994), although the mechanisms by which it may affect cell adhesion and migration remain unclear.

We describe here a new and complex interplay between N-cadherin adhesive engagement and FGFR1 activation positively regulating the strength of cadherin-dependent cell-cell adhesion and decreasing cell migration on N-cadherin surfaces. To mimic N-cadherin-dependent neural or cancer cells migration over neighboring cells, we set up a model system of isolated N-cadherin or N-cadherin/FGFR1 expressing cells migrating on recombinant N-cadherin-coated lines. FGFR1 expression dramatically blocked N-cadherin-dependent single cell migration. This inhibition of migration was associated to an increased cell spreading due to a strengthening of N-cadherin-mediated adhesion. Indeed, FGFR1 expression led to the reinforcement of N-cadherin adhesion as demonstrated by the increased recruitment and stabilization of junctional N-cadherin. We do not know if FGFR1 regulates directly the “cis” or “trans”- clustering of N-cadherin that may affect its stability at the plasma membrane (Mege and Ishiyama, 2017). However, this stabilization was associated to an increased resistance of cell-cell contacts to calcium depletion, to an increase in the coupling of cadherin complexes to the actin treadmilling and to a rise in the mechanical strength of cell contacts. Indeed, the rupture force of N-cadherin-mediated bead-cell contacts was significantly increased by FGFR1 expression. Notice that rupture forces measured here were in the same range than those reported for doublets of N-cadherin expressing S180 cells (7.7 ± 1.4 nN) (Chu et al., 2006).

Altogether, our data strongly support the hypothesis that FGFR1 blocks cell migration on N-cadherin surfaces as a result of a major N-cadherin adhesion strengthening. This

bioRxiv preprint doi: https://doi.org/10.1101/465930; this version posted November 8, 2018. The copyright holder for this preprint (which was not certified by peer review) is the author/funder. All rights reserved. No reuse allowed without permission.

behavior is reminiscent of the reported biphasic relationship between the strength of integrin mediated adhesion and migration of cells on fibronectin (Palecek et al., 1997; Peyton and Putnam, 2005). Cell migration is enhanced with increasing adhesion up to a threshold, above which further increase in adhesion acts to the detriment of migration. Accordingly, cells expressing only N-cadherin were poorly spread and supported cycles both adhesion and deadhesion, allowing them to migrate and invert their polarity whereas cells expressing also FGFR1 remained tightly spread on the cadherin-coated substrate preventing any movement. Interestingly, pharmacological treatments altering actomyosin contraction and actin dynamics in the lamellipodium fully blocked the migration of N-cadherin expressing cells but significantly stimulated the migration of cells expressing FGFR1 likely by having in addition a destabilizing effect on cadherin-based adhesion as expected from the contribution of actomyosin-based contractility to the stability and strength of cadherin contacts (Mege and Ishiyama, 2017). Accordingly, the positive effect of FGFR signaling on the migration of neuronal cell growth cones (Boscher and Mege, 2008; Williams et al., 1994) may be related to the intrinsic weak adhesion of neuronal cells.

The increase in cell adhesion and reduction of migration induced by FGFR1 required the kinase activity of the receptor. Although we cannot exclude that FGFR1 could be activated by FGFs autonomously produced by HEK cells, we provide evidence here that N-cadherin engagement stimulates the activation of FGFR1, in agreement with previous observations made in neuronal cells (Boscher and Mege, 2008; Utton et al., 2001). We further provide evidence that the presence of N-cadherin strongly decreases the mobility of FGFR1 at cell-cell contacts suggesting that the receptor was trapped in higher order complexes or membrane domains. Interestingly, this effect is N-cadherin specific as junctional FGFR1 stabilization was not observed while co-expressed with E-cadherin. We confirmed by co-immunoprecipitation but also using purified proteins that FGFR1 and N-cadherin interact through their extracellular domain. This may be essential for FGFR1 activation: decreasing the mobility of the receptor and/or increasing its local density at cell-cell contacts may stimulate its dimerization and cross phosphorylation independently of FGF binding. The cellular responses reported in this study, including the regulation of N-cadherin trafficking and of the mechanocoupling between N-cadherin and actin require the activation of the receptor.

The sustained activation of FGFR1 significantly increased N-cadherin levels at the plasma membrane and we further observed that FGFR1 had an inhibitory effect on N-

bioRxiv preprint doi: https://doi.org/10.1101/465930; this version posted November 8, 2018. The copyright holder for this preprint (which was not certified by peer review) is the author/funder. All rights reserved. No reuse allowed without permission.

cadherin endocytosis. The level of expression of the catenin p120 has been reported to stabilize N-cadherin at the cell-cell contacts by preventing cadherin internalization (Davis et al., 2003), making it a good candidate to regulate N-cadherin trafficking, but we did not observed any change in the cellular or cadherin-associated levels of p120. However, FGFR1 expression decreased the level of phosphorylation of p120 in cadherin complexes. Since it has been reported that the phosphorylation of this catenin may induce its dissociation from cadherins allowing endocytosis of the latter (Ireton et al., 2002), the negative effect of FGFR1 on p120 phosphorylation may be a relay to stabilize junctional N-cadherin and/or prevent N-cadherin endocytosis. Accordingly, we found that a mutant of N-cadherin impaired for it binding to p120 was not stabilized at cell-cell junctions, as measured by FRAP. Cells expressing this protein together with FGFR1 poorly spread on N-cadherin while migrating at high speed. These data suggest that p120 is involved in the regulation of N-cadherin stabilization at cell adhesion sites by FGFR1. Altogether, the decreased in N-cadherin endocytosis is directly linked to the migratory properties of cells on N-cadherin substrates. It is important here to recall that in the case of the radial migration of cortical neurons *in vivo*, efficient migration on radial glia requires an active recycling of N-cadherin in neurons (Franco et al., 2011; Jossin and Cooper, 2011; Kawauchi et al., 2010). In this system, both the blockade of N-cadherin recycling and N-cadherin overexpression induced abnormal stabilization of cell-cell contacts and impaired cell migration. .

We unravelled an involvement of Src family kinases in the cellular response to FGFR1 expression. Blocking pharmacologically Src family kinase activities reverted the effect of FGFR1 on cell spreading and migration on N-cadherin surfaces. We also noticed that FGFR1 induced a rise in N-cadherin-associated activated Src. Even if p120 is a recognized Src substrate, it is unlikely that Src directly phosphorylates p120 at cell-cell contacts since we observed at the same time an increased in Src activation and a decrease in p120 phosphorylation associated to N-cadherin upon FGFR1 activation. The inhibition of Src had a significant blocking effect on the stabilization of N-cadherin at cell-cell contacts induced by FGFR1. Src was also involved in the mechanocoupling between N-cadherin complexes and the actin retrograde flow.

Taken together, these data reveal the existence of a signaling pathway controlled by FGFR1 and N-cadherin to regulate cadherin-dependent cell-cell adhesion and cell migration. FGFR1 and N-cadherin are co-recruited and co-stabilized at the cell-cell adhesions. This leads to sustained activation of FGFR1, which in turn promotes N-cadherin accumulation at the

bioRxiv preprint doi: https://doi.org/10.1101/465930; this version posted November 8, 2018. The copyright holder for this preprint (which was not certified by peer review) is the author/funder. All rights reserved. No reuse allowed without permission.

plasma membrane, strengthens N-cadherin mediated cell-cell contacts and N-cadherin mechanocoupling to actin. Adhesion between migrating cells and N-cadherin-expressing cellular substrates is increased therefore decreasing cell migration. This mechanism could be used by cancer cells to engraft to the vessel wall or the host tissue. In less adherent cells, such as neurons or in other places for cancer cells or considering different type of cancer cells, depending on the level of expression of N-cadherin and the dynamics of the actomyosin cytoskeleton, the same pathway may also promote single or collective cell migration.

bioRxiv preprint doi: https://doi.org/10.1101/465930; this version posted November 8, 2018. The copyright holder for this preprint (which was not certified by peer review) is the author/funder. All rights reserved. No reuse allowed without permission.

Materials and Methods

Plasmid constructions

The construct encoding GFP-FGFR1 (FGFR1 tagged with GFP at its carboxy-terminal extremity) was obtained using as a template pMIRB-FGFR1-Myc plasmid (gift from D. Ornitz, University of Washington), which encodes for the mousse fgfr1-IIIc full length sequence. By performing polymerase chain reactions (PCR) using sets of appropriate primers, (i) HindIII restriction site was introduced at 5' extremity (5'-GCGAAGCTTACCATGTGGGGCTGGAAGTGCC-3') while, (ii) stop codon was abolished, and AgeI restriction site was introduced at 3' extremity (5'-GCGACCGGTGGGCGCCGTTTGAGTCCACTGTT-3') of the FGFR1 encoding sequence. Resulting PCR product was subcloned into the pEGFP-N1 vector using the HindIII and AgeI restriction sites.

The constructs encoding Flag-FGFR1 (FGFR1 tagged with a flag tag at its carboxy-terminal extremity) was obtained using also as a template pMIRB-FGFR1-Myc plasmid, by performing polymerase chain reactions (PCR). Using sets of appropriate primers, (i) NheI restriction site was introduced at 5' extremity (5'-GCGGCTAGCACCATGTGGGGCTGGAAGTGCC-3') while , (ii) a Flag tag encoding sequence and PmeI restriction site was introduced at 3' extremity (5'-CGCGTTTAAACTCACTTATCGTCGTCATCCTTGTAATCGGCGGCCCCGCGCCGTTT GAGTCCACTGTT-3') of the FGFR1 encoding sequence. Resulting PCR product was subcloned into the pcDNA3.1 hygro(-) vector using the NheI and PmeI restriction sites.

Cell culture, transient cell transfection and generation of stable cell lines

HEK (Human Embryonic Kidney) and C2C12 mouse myoblastic cells were grown in DMEM medium supplemented with 10% fetal bovine serum (FBS), 2 mM L-Glutamine, 100 IU of penicillin, 100 µg/mL streptomycin, at 37°C in the presence of 5% CO_2. HEK cells were transiently electroporated with the plasmids encoding for dsRed-fused wild type N-cadherin (dsRed-Ncad), or N-cadherin 3A mutated in the p120 binding site (dsRed-NcadAAA) (Bard et al., 2008; Thoreson et al., 2000) and/or with a plasmid coding for GFP- or Flag- FGFR1. Electroporation was performed with the Amaxa Cell Line Nucleofector (kit V, program X-032). To generate dsRed-Ncad, GFP-FGFR, dsRed-Ncad/GFP-FGFR dsR-Ncad/Flag-FGFR stable HEK cell lines, transfected cells were grown under a selection

bioRxiv preprint doi: https://doi.org/10.1101/465930; this version posted November 8, 2018. The copyright holder for this preprint (which was not certified by peer review) is the author/funder. All rights reserved. No reuse allowed without permission.

pressure of 200 µg/mL of Hygromycin B, 1 mg/mL of Geneticin or both. Drug resistant cells were then sorted out by FACS (Influx 500 Cytopeia/BD-Biosciences) subcloned and further maintained with half of concentration of antibiotic pressure.

Drug treatments

The FGFR's kinase activity inhibitor, PD173074 (Sigma, 20 nM final concentration) and the Src family proteins inhibitor, PP2 (Abcam, 100 nM final concentration) were added in the medium 30 minutes prior the beginning and maintain throughout the experiments. Hydroxy-dynasore (Sigma, 100 nM final concentration) was incubated for 1 hour.

Protein extraction and co-immunoprecipitation

Proteins were extracted from 5-6 x 10^6 cells. Cell cultures were rinsed in ice-cold PBS, detached with non-enzymatic detaching solution (Cell Dissociation Solution Non-enzymatic 1x, Sigma) and centrifuged at 200 rcf for 7 minutes. Cell pellets were suspended in lysis buffer (10 mM TrisCl pH 7.5; 150 mM Nacl; 0.5 mM EDTA; 0.5% Triton) on ice. Cells were then passed slowly 10 times through a 26 gauge needle and left on ice for 1 hour with extensive pipetting every 10 minutes. Lysates were cleared by centrifugation at 20000 rcf for 10 min at 4°C. GFP-tagged proteins were then immunoprecipitated using magnetic GFP-Trap®-M beads accordingly to manufacturer instructions (Chromotek). Briefly, 25 µl of GFP-Trap®-M beads were washed 3 times with the wash buffer (10 mM Tris H-Cl pH 7.5, 150 mM NaCl, 0.5 mM EDTA). Fifteen µl of beads were added to 300 µl of protein extracts diluted in lysis buffer and tumbled end-over-end for 1 hour at 4°C. Beads were then magnetically separated, washed 3 times with the wash buffer, suspended in 100 µl 2x sample buffer plus reducing agent (NuPAGEr, Invitrogen) and boiled at 95°C for 10 minutes to recover bound proteins. Proteins from the input and bound proteins were subjected to SDS-PAGE electrophoresis using Bis-Trisacrylamide 4%-12% NuPAGE gels (Invitrogen) then transferred on nitrocellulose membranes (0.45 µm, GE Healthcare). Membranes were blocked with 5% nonfat milk and incubated with the adequate primary antibodies : mouse anti-GFP antibody (1:1000, Roche); anti-Ncadherin antibody 1:500, Cell Signaling; anti-p120 antibody 1:1000, Santa-Cruz; rabbit anti-phosphotyrosine 228 p120 antibody (1:500, Abcam); mouse anti-α-tubulin antibody (1:5000, Sigma); mouse anti-phosphotyrosine antibody clone 4G10 (1:500, Millipore), rabbit anti-Src (1:1000, Cell Signaling) and rabbit anti-phospho-Src (Tyr416) (1/1000, Cell Signaling) and then with IRDye-coupled secondary antibodies

bioRxiv preprint doi: https://doi.org/10.1101/465930; this version posted November 8, 2018. The copyright holder for this preprint (which was not certified by peer review) is the author/funder. All rights reserved. No reuse allowed without permission.

(Rockland). The membranes were scanned using Odyssey Imaging System (LY-COR Biosciences).

FGFR activation and Ca^{2+} switch assay

C2C12 cells cultures were starved in serum-free medium 24 hours, then treated for 5 minutes with 1ng/ml of FGF2 (homemade, produced according to (Ke et al., 1992). For the Ca^{2+} switch assay, EGTA was added at 4 mM for 20 minutes on starved cultures. After three washes with PBS without Ca^{2+} and Mg^{2+}, cells were incubated for 10 minutes in DMEM culture medium supplemented with 5 mM of $Ca^{2+}Cl^{2-}$. The FGFR inhibitor PD17430 was added 20 minutes before and maintained during the whole experiment. Cells were then subjected to protein extraction followed by immunobloting using rabbit anti-Erk1/2 antibodies (1:1000, Sigma) and mouse anti-P-erk1/2 (1/1000, Upstate Biotechnology).

Surface biotinylation and endocytosis assay

Cell cultures were chilled down to 4°C by three washes with cold PBS/Mg^{2+}/Ca^{2+} then labelled with 1 mg/ml of NHS-SS biotin (Pierce) diluted in PBS/Mg^{2+}/Ca^{2+} for 12 minutes at 4°C under gentle rocking. The biotinylation reagent was quenched by two washes with PBS/Mg^{2+}/Ca^{2+} containing 50 mM Glycine and 0.5% BSA at 4°C. Cells were then washed twice in cold PBS/Mg^{2+}/Ca^{2+} and lysed. Biotinylated plasma membrane proteins were then separated by precipitation with streptavidin-coated magnetic beads (Pierce).

For endocytosis biochemical assays, cell surface biotinylation and quenching at 4°C were performed as above. Then, the cold PBS/Mg^{2+}/Ca^{2+} was replaced by pre-warmed culture medium and the culture dishes were returned at 37°C to allow endocytosis to resume for 40 minutes. Cells were then chilled down with cold PBS/Mg^{2+}/Ca^{2+} and bound biotin remaining at the cell surface was cleaved by incubating with 50 mM Glutathione in 75 mM NaCl, 10 mM EDTA, pH 7.5 for 15 minutes under gentle agitation. After three washes with PBS/Mg^{2+}/Ca^{2+}, cells were lysed and protein extracts were subjected to precipitation with streptavidin-coated beads or with GFP-Trap®-M beads (Chromotek). Immunoprecipitates were resolved by SDS-PAGE electrophoresis and immunoblotting using anti-N-cadherin antibodies.

bioRxiv preprint doi: https://doi.org/10.1101/465930; this version posted November 8, 2018. The copyright holder for this preprint (which was not certified by peer review) is the author/funder. All rights reserved. No reuse allowed without permission.

Cell Fractionation

Cells grew at 80% confluence were washed 3 times with ice-cold PBS then scraped in 500 µl of detergent-free buffer **(**20 mM Tris-Cl pH 7.4, 100 mM NaCl, 2 mM MgOAc, 5 mM KCl, 10 mM GTP + protease inhibitor cocktail- both added fresh). Cells were dounced 35 times with a 26-gauge needle on ice and centrifuged at 450 rcf, 10mn. Pellets containing nuclei was discarded. Supernatants were collected and centrifuged at 20000 rcf for 30 minutes. The supernatants, (cytosolic fraction) were collected. The pellets (membrane fraction) were rinsed with 1ml of lysis buffer then spun at 20000 rcf for 30 minutes. The pellets were re-suspended in 180 µl of detergent-free buffer supplemented with 1% NP-40 and incubated on ice for 1 hour while mixing every 10 minutes. The fractions were resolved by SDS-PAGE electrophoresis and immunoblotting using anti-GFP antibodies (1:500, Roche), anti-N-cad antibodies (1:500, Cell Signaling) and anti-p120 antibody (1:1000, Santa-Cruz).

Fixed cell imaging

Cell cultures were fixed at room temperature in PBS 4 % formaldehyde for 15 minutes. Preparations were then mounted in Mowiol, 90% glycerol. Images were acquired with a Leica TCS SP5 inverted confocal microscope AOBS tandem, equipped with a 63x oil objective (N.A=1.4), controlled by LAS AF (Leica System).

Ncad-Fc line guided cell migration

Patterned silicon microcontact stamps bearing 10 µm width lines spaced of 70 µm were prepared by soft lithography according to a protocol derived from (Vedula et al., 2014). Patterned stamps were incubated with 1 µg/cm^2 anti-human IgG (Jackson Immunoresearch), pressed on non-culture treated petri dishes or on cleaned glass coverslip previously activated by deep UV (Jelight, 4 X 60W, 15 minutes). Microcontact printed surfaces were then passivated by incubation for 1 hour with 1% Pluronics F-127 (Sigma) diluted in distilled water, followed by 3 washes with PBS. Surfaces were incubated with 1µg/µm^2 hNcad-Fc (R&D) for 2 hours at room temperature then washed three times with PBS. Cells in culture were then dissociated on non-enzymatic detaching solution (Cell Dissociation Solution Non-enzymatic 1x, Sigma), seeded (10^5cells/200µl/cm^2) on these arrays of Ncad-Fc-coated lines and allowed to adhere for 1-2 hours in culture medium containing 1 µg/mL of mytomycin, before non-adhesive cells were gently washed off. Cells were imaged live or fixed 18 hours

bioRxiv preprint doi: https://doi.org/10.1101/465930; this version posted November 8, 2018. The copyright holder for this preprint (which was not certified by peer review) is the author/funder. All rights reserved. No reuse allowed without permission.

after seeding. For live imaging, Images were acquired with a 10 X objective, every 6 minutes during 24 hours under controlled environment (37° C, 5% CO_2, Biostation Nikon). Manual tracking of individual cells was performed with the MTrackJ plugin. Individual trajectories were positioned on an orthonormal axis with the coordinates of the cells at t_0 = (0:0). The displacements and mean cell speed were then extracted for each condition and plotted versus time and cell area, respectively.

Cell-cell contact disruption assay

Glass or plastic surfaces were microcontact printed with silicon stamps bearing 200 µm fibronectin-coated squares as described in (Vedula et al., 2014). Cells were seeded on the patterned surfaces in the presence of 10 µg/mL mitomycin. After 1 h, unattached cells and mitomycin were washed out and preparations were returned to the incubator overnight. Preparation were processed for live image directly after addition of 5 mM of EGTA solution or fixed after 15 minutes of EGTA treatment. Live images were acquired at 20 x objective, every 30 seconds for 30 minutes under a controlled environment (37°C, 5% CO_2, type Inverted Olympus IX81, camera CoolSnap HQ^2) using MetaMorph. Fixed samples were acquired with the same microscope and camera, using 20 x and 60 x objectives.

Cell doublets on fibronectin-coated line assay

Stable dsR-Ncad and dsR-Ncad/Flag-FGFR HEK cell lines were transiently transfected with GFP-p120 or lifeact-GFP and seeded on fibronectine-coated-10 µm width lines prepared as in (Vedula et al., 2014), and let adhere for 1-2 hours. Samples were gently washed and returned to the incubator overnight. cell doublets were chosen to image in red-phenol-free DMEM supplemented with 10% serum every minutes during 1 hour under a controlled temperature and CO_2 environment (37°C, 5% CO_2, 40x oil objectives (N.A = 1.4), Spinning disk CSU22). Localizations of fluorescent proteins relative to the junction end were analysed using ImageJ for mask creating and Matlab for intensity calculation. All the fluorescence images were background-subtracted before quantification. The cells shape were detected by segmenting the fluorescence intensity image using Otsu method and converted into binary mask images with values outside the cell set to zero. The cell lengths were normalized to unity in the strip direction (x direction). For each individual cell, the fluorescence intensities within the cell mask along the x direction were averaged in the y direction (perpendicular to the strip direction) and projected in the x direction. The average intensity curves were normalized by the whole cell intensity and plotted against the

bioRxiv preprint doi: https://doi.org/10.1101/465930; this version posted November 8, 2018. The copyright holder for this preprint (which was not certified by peer review) is the author/funder. All rights reserved. No reuse allowed without permission.

normalized distance to the junction end. The average intensities in the x direction from multiple cells with the same experimental condition were calculated and an average curve was then created using Matlab function smooth by filtering with locally quadratic regression using a moving window of size 5. The overall behaviour of each group of multiple cells was then represented by one single curve.

Fluorescence Recovery after Photobleaching

Dual wavelength fluorescence recoveries after photobleaching (FRAP) was performed at 37°C on stably transfected Ncad, FGFR or Ncad/FGFR expressing cells, as well as on transiently transfected Ecad and Ecad/FGFR expressing cells. FRAP was performed using a Leica TCS SP5 confocal microscope equipped with a 40 X immersion objective (N.A=1.4) and carried out by setting the double scanning mode at 560 nm for dsRed and 480 nm for GFP and the image format to 256 $_X$ 256 pixels. After 3 prebleach scans (0.347 sec), a 20 x 40 µm ROI over the cell-cell contact was bleached with laser at full power by performing repeated scans. Recovery was recorded by imaging with low laser power every 0.347 sec (20 scans) then every 2 sec (20 scans) and finally every 10 sec (20 scans). The normalized recovery of fluorescence was expressed as a ratio of prebleach fluorescence after correction for photobleaching as reported previously (Strale et al., 2015). Normalized fluorescence recovery in function of time curves were fitted with a one-term exponential equation using GraphPad Prism 5.01 software (one-phase decay non-linear regression function$_5$), allowing to extract a plateau value representing the fraction of diffusion-limited molecules (mobile fraction) and a recovery half-time ($t_{1/2}$) as a proxy of the apparent diffusion coefficient of diffusion-limited molecules (Thoumine et al., 2006).

Flow Cytometry

Cells were detached using non-enzymatic detaching solution (Cell Dissociation Solution Non-enzymatic 1x, Sigma), centrifuged at 200 rcf during 4 minutes, resuspended in culture medium and returned to the incubator for 10 minutes favoring moderate cell-cell adhesion in suspension. Cells were centrifuged again at 200 rcf for 4 minutes, fixed in 4% formaldehyde for 15 minutes, washed 3 times in PBS, incubated in the presence of 0.1% Dapi in PBS-BSA 0.1 % for 5 minutes, washed again then imaged under flow using ImageStream X (Amnis, Proteigene) set with the 405, 488, 560-nm laser and 480-560 filter. Data were analyzed using the IDEAS software (Amnis, Proteigene) focusing on singulets for the quantifications of internal pool and on doublets for cell-cell accumulation of DsRed-Ncad

bioRxiv preprint doi: https://doi.org/10.1101/465930; this version posted November 8, 2018. The copyright holder for this preprint (which was not certified by peer review) is the author/funder. All rights reserved. No reuse allowed without permission.

fluorescence. For internal fluorescence quantification, regions corresponding to the total cell surface, the internal cell area and the cell membrane area were extracted from bright field images of singulets. Briefly, the morphology mask was applied to bright field images. Then, 4 pixels were evenly eroded from the border of the mask in order to exclude the cell membrane from the mask. The resulting mask was applied to the fluorescence channel. The internalization feature was then applied to the final mask in order to calculate the internalization score. Internalization score per surface unit was defined as the ratio of internal fluorescence intensity per surface unit over the overall intensity per surface unit in the whole cell expressed on a logarithmic range.

The N-cadherin recruitment at the cell-cell interface was determined on doublet populations. Regions corresponding to the total cell surface and the cell-cell interface were extracted from bright field images and dapi staining, respectively. The 4 pixels interface mask was determined as a region centered at the dimmest pixel between the 2 nuclei (dapi). The interface mask was applied to the bright field channel to determine the surface area of the cell-cell contacts in the doublets, then to the fluorescence channel to count the intensity of Ncad staining at the cell-cell contact. Results were expressed as fluorescence intensity per surface unit. The Bright Detail Intensity (BDI) was determined by a feature of IDEAS analysis assessing for the intensity of bright spots that have radii of 4 pixels after correction for background staining. Data acquisition was performed for 1.5 x 10^5 cells for each condition and repeated 4 times.

Magnetic tweezers

A homemade magnetic tweezer was the source of the magnetic field gradient used to pull Ncad-Fc coated paramagnetic microbeads attached to the cells. The magnetic microneedle device was made of a 5 cm long stainless steel sewing needle glued to the top of permanent neodymium iron boron (NeFeB) surface surrounded by an aluminium rod. The montage was assembled on a micromanipulator (MP-285, Sutter Instrument) at a 30°C vertical angle, and the tip initially aligned at 600 µm from the centre of the observation field. The whole device was mounted on an inverted microscope (Olympus IX 81) equipped with a 40 x phase contrast air objective and a CCD camera (CoolSnap HQ^2) operating in the burst mode (frequency of 15 frames/s for 2 minutes). The micromanipulator allowed translational movement across all three axes with nanometer precision to position the magnetic field in the vicinity of beads. The distance between the tip of needle and detached bead was measured with imageJ.

bioRxiv preprint doi: https://doi.org/10.1101/465930; this version posted November 8, 2018. The copyright holder for this preprint (which was not certified by peer review) is the author/funder. All rights reserved. No reuse allowed without permission.

The force applied to the bead is decreasing exponentially with the distance to the magnetic rod. To calibrate the magnetic force with is a function of the distance between the needle tip and the bead, 4.5 µm beads ware placed in a 100 % polyethylenglycol solution (Mn 700, Sigma) at various distances of the needle and the bead motion was tracked by video microscopy. The instantaneous horizontal bead velocity (v) was extracted using ImageJ tracking. The force applied on the bead (F) was calculated respecting Stokes equation*:* $v = F/6\pi\eta r$, where η is the dynamic fluid viscosity (for PEG Mn700: η = 25 Pa.s at 25°C) and r is the radius of the bead.The calibration was performed ten times and the forces versus distance data were regressed to an exponential equation.

For the measurement of the rupture force of N-cadherin-mediated bead-cell contacts, Ncad or Ncad/FGFR cells seeded on 10 µm-width fibronectin coated lines were incubated with 4.5 µm magnetic Ncad-Fc coated beads for 30 minutes, then unbound beads were washed out. The magnetic microneedle was approached while cells and the moving tip were imaged in phase contrast (every 10 milliseconds during 2 minutes).

Production and biotinylation of soluble FGFR1 extracellular domain

The soluble FGFR1 extracellular domain (FGFR1-ST) used here corresponds to amino acids 120 to 368 of the FGFR1IIIc comprising the acid box and immunoglobulin loops D2 and D3 with a poly-histidine-tail sequence followed by a thrombin cleavage site at the N-terminus and a Factor Xa cleavage site followed by a Strep-Tag II sequence at the C-terminus and is termed FGFR1-ST. This protein was produced in CHO cells and is heavily N-glycosylated (Duchesne et al., 2006). For biotinylation, 2 µL of sodium periodate at 0.5 M freshly resuspended in water was added to 28 µL of purified FGFR1-ST at 16 µM in PBS supplemented by 0.01% of tween (PBS-T). The mixture was left incubated 1 hour in the dark. Excess sodium periodate was then removed using nanosep 30 kDa centrifugal device following the manufacturer recommendation and using PBS-T as exchange buffer. Purified periodated FGFR1-ST was recovered in 50 µL of PBS-T and 1.5 µL of biotin-LC-hydrazyde at 135 mM in DMSO was then added. The reaction was left incubated overnight at RT and then kept 6 hours at 4°c. Excess biotin-Lc-Hydrazide was removed using nanosep 30 kDa centrifugal device following the manufacturer recommendation and PBS-T as exchange buffer. Biotinylated FGFR1-ST was recovered in 200 µL of PBS-T and kept at -20° c. Its concentration was estimated at 1.14 µM by measurement of the absorbance at 280 nm ($\varepsilon_{280\ nm}$ of 47424 $mole^{-1}.L.cm^{-1}$).

Optical biosensor experiments

bioRxiv preprint doi: https://doi.org/10.1101/465930; this version posted November 8, 2018. The copyright holder for this preprint (which was not certified by peer review) is the author/funder. All rights reserved. No reuse allowed without permission.

Streptavidin (Sigma, 50 µl at 2.5 mg/mL) was immobilised on aminosilane surfaces using bissulfosuccinimidyl suberate (BS^3, Perbio, 1 mM) as the cross linker following the manufacturer's recommendations (NeoSensors, Sedgefield, UK). Surface was washed 5 times with 80 µL of Pi buffer (10 mM sodium phosphate buffer pH 7.2) and then incubated 3 min in 2M Tris-Hcl, pH 8 to stop the cross-linking reaction. Three washes with 80 µL of Pi buffer and then of PBST were then performed before the addition of 25 µL of biotinylated FGFR1-ST at 1.14 µM. The reaction was left incubated for 4 to 6 hrs at RT and then overnight at 4°C. Cuvette was then cleaned by washing 3 times with 50 µL of PBST, Nacl 2 M in Pi buffer, PBST, HcL 20 mM and then PBST again.

Binding assays were carried out in TNC buffer (Tris-Hcl 20 mM pH 7.5, Nacl 150 mM, $Cacl_2$ 2 mM and Tween-20 0.02%). A single binding assay consisted of adding 0.5 to 6 µL of purified Ncad-Fc to a cuvette containing 19 to 24.5 µL or 24 to 29.5 µL of TNC. The association reaction was followed until binding was at least 90 % of the calculated equilibrium value, usually between 150 s and 230 s. The cuvette was then washed three times with 50 µL TNC to initiate the dissociation of bound Ncad-Fc. Regeneration of the surface between each binding assay was performed by washing 3 times with 50 µL 2 M NaCl in Pi buffer, TNC, 20 mM HCl, and then TNC, which removed 98 % to 100 % of bound Ncad-Fc. Binding parameters were calculated using the non-linear curve fitting program FASTFit (NeoSensors). Each binding assay yielded four binding parameters, which are the slope of initial rate of association, the on-rate constant (k_{on}) and the extent of binding, all calculated from the association phase, and the off-rate constant (k_{off}, equivalent to the dissociation rate constant, k_{diss}), calculated from the dissociation phase. Biosensor experiments were carried out 4 times on 3 different FGFR1-ST-derivatized surfaces. The determination of binding kinetics in optical biosensors was prone to second phase binding sites at high concentration of Ncad-Fc. Thus, limiting amounts of ligand were immobilised on the sensor surface, whereas the slope of initial rate, k_{on} and the extent of binding were only determined at low concentrations of ligate (3 different experiments), and k_{off} was measured at higher concentrations of ligate (2 different experiments), to avoid steric hindrance and rebinding artefacts. A single site model was used to calculate all binding parameters. The dissociation constant (K_D) was calculated both from the ratio of the k_{diss} and k_{ass} and from the extent of binding, to provide an estimate of the self-consistency of the results.

bioRxiv preprint doi: https://doi.org/10.1101/465930; this version posted November 8, 2018. The copyright holder for this preprint (which was not certified by peer review) is the author/funder. All rights reserved. No reuse allowed without permission.

Acknowledgement

This work was supported by grants from CNRS, ARC foundation (contract number: PJA 20151203185), Human Frontier Science Program (HFSP grant RPG0040/2012),European Research Council under the European Union's Seventh Framework Program (FP7/2007-2013) / ERC grant agreements n° 617233 (BL), Agence Nationale de la Recherche (ANR 2010 Blan1515) and NUS-USPC exchange program. TN was supported by a HFSP grant RPG0040/2012 then by FRM (Fondation pour la Recherche Médicale) and Labex WhoAmI. We would like also to thank all present and past member of the Cell Adhesion & Mechanics lab at the Institute Jacques Monod for constant support and exchange. We thank Region Ile de France (E539) and Ligue contre le Cancer (R03/75-79) for the acquisition of the equipments. We thank C. Murade and M. Yao for held with magnetic tweezer experiment. C.M. was supported by Fondation pour la Recherche Médicale (FDT20150532600) and L.D. by the Association pour la Recherche contre le Cancer (Fondation ARC, P2009 CDD POST-DOC). We thank O.Thoumine and R. Horwitz for their kind gift of NcadAAA and FGFR1 encoding plasmids, respectively. We acknowledge the ImagoSeine core facility of the Institut Jacques Monod, member of IBiSA and France-BioImaging (ANR-10-INBS-04) infrastructures.

bioRxiv preprint doi: https://doi.org/10.1101/465930; this version posted November 8, 2018. The copyright holder for this preprint (which was not certified by peer review) is the author/funder. All rights reserved. No reuse allowed without permission.

References

Bard, L., Boscher, C., Lambert, M., Mege, R. M., Choquet, D. and Thoumine, O. (2008). A molecular clutch between the actin flow and N-cadherin adhesions drives growth cone migration. *J Neurosci* **28**, 5879-90.

Bixby, J. L. and Zhang, R. (1990). Purified N-cadherin is a potent substrate for the rapid induction of neurite outgrowth. *J Cell Biol* **110**, 1253-60.

Boscher, C. and Mege, R. M. (2008). Cadherin-11 interacts with the FGF receptor and induces neurite outgrowth through associated downstream signalling. *Cell Signal* **20**, 1061-72.

Brittis, P. A., Silver, J., Walsh, F. S. and Doherty, P. (1996). Fibroblast growth factor receptor function is required for the orderly projection of ganglion cell axons in the developing mammalian retina. *Mol Cell Neurosci* **8**, 120-8.

Carmeliet, P. and Collen, D. (2000). Molecular basis of angiogenesis. Role of VEGF and VE-cadherin. *Ann N Y Acad Sci* **902**, 249-62; discussion 262-4.

Chen, X., Kojima, S., Borisy, G. G. and Green, K. J. (2003). p120 catenin associates with kinesin and facilitates the transport of cadherin-catenin complexes to intercellular junctions. *J Cell Biol* **163**, 547-57.

Chu, W. C., Lee, Y. M. and Henry Sun, Y. (2013). FGF /FGFR signal induces trachea extension in the drosophila visual system. *PLoS One* **8**, e73878.

Chu, Y. S., Eder, O., Thomas, W. A., Simcha, I., Pincet, F., Ben-Ze'ev, A., Perez, E., Thiery, J. P. and Dufour, S. (2006). Prototypical type I E-cadherin and type II cadherin-7 mediate very distinct adhesiveness through their extracellular domains. *J Biol Chem* **281**, 2901-10.

Ciruna, B. and Rossant, J. (2001). FGF signaling regulates mesoderm cell fate specification and morphogenetic movement at the primitive streak. *Dev Cell* **1**, 37-49.

Ciruna, B. G., Schwartz, L., Harpal, K., Yamaguchi, T. P. and Rossant, J. (1997). Chimeric analysis of fibroblast growth factor receptor-1 (Fgfr1) function: a role for FGFR1 in morphogenetic movement through the primitive streak. *Development* **124**, 2829-41.

Davis, M. A., Ireton, R. C. and Reynolds, A. B. (2003). A core function for p120-catenin in cadherin turnover. *J Cell Biol* **163**, 525-34.

Debiais, F., Lemonnier, J., Hay, E., Delannoy, P., Caverzasio, J. and Marie, P. J. (2001). Fibroblast growth factor-2 (FGF-2) increases N-cadherin expression through protein kinase C and Src-kinase pathways in human calvaria osteoblasts. *J Cell Biochem* **81**, 68-81.

Deng, C. X., Wynshaw-Boris, A., Shen, M. M., Daugherty, C., Ornitz, D. M. and Leder, P. (1994). Murine FGFR-1 is required for early postimplantation growth and axial organization. *Genes Dev* **8**, 3045-57.

Derycke, L. D. and Bracke, M. E. (2004). N-cadherin in the spotlight of cell-cell adhesion, differentiation, embryogenesis, invasion and signalling. *Int J Dev Biol* **48**, 463-76.

Duchesne, L., Tissot, B., Rudd, T. R., Dell, A. and Fernig, D. G. (2006). N-glycosylation of fibroblast growth factor receptor 1 regulates ligand and heparan sulfate co-receptor binding. *J Biol Chem* **281**, 27178-89.

Franco, S. J., Martinez-Garay, I., Gil-Sanz, C., Harkins-Perry, S. R. and Muller, U. (2011). Reelin regulates cadherin function via Dab1/Rap1 to control neuronal migration and lamination in the neocortex. *Neuron* **69**, 482-97.

Gavard, J., Marthiens, V., Monnet, C., Lambert, M. and Mege, R. M. (2004). N-cadherin activation substitutes for the cell contact control in cell cycle arrest and myogenic differentiation: involvement of p120 and beta-catenin. *J Biol Chem* **279**, 36795-802.

Giannone, G., Mege, R. M. and Thoumine, O. (2009). Multi-level molecular clutches in motile cell processes. *Trends Cell Biol* **19**, 475-86.

Giannotta, M., Trani, M. and Dejana, E. (2013). VE-cadherin and endothelial adherens junctions: active guardians of vascular integrity. *Dev Cell* **26**, 441-54.

bioRxiv preprint doi: https://doi.org/10.1101/465930; this version posted November 8, 2018. The copyright holder for this preprint (which was not certified by peer review) is the author/funder. All rights reserved. No reuse allowed without permission.

Gumbiner, B., Stevenson, B. and Grimaldi, A. (1988). The role of the cell adhesion molecule uvomorulin in the formation and maintenance of the epithelial junctional complex. *J Cell Biol* **107**, 1575-87.

Huttenlocher, A. and Horwitz, A. R. (2011). Integrins in cell migration. *Cold Spring Harb Perspect Biol* **3**, a005074.

Ireton, R. C., Davis, M. A., van Hengel, J., Mariner, D. J., Barnes, K., Thoreson, M. A., Anastasiadis, P. Z., Matrisian, L., Bundy, L. M., Sealy, L. et al. (2002). A novel role for p120 catenin in E-cadherin function. *J Cell Biol* **159**, 465-76.

Jossin, Y. and Cooper, J. A. (2011). Reelin, Rap1 and N-cadherin orient the migration of multipolar neurons in the developing neocortex. *Nat Neurosci* **14**, 697-703.

Kadowaki, M., Nakamura, S., Machon, O., Krauss, S., Radice, G. L. and Takeichi, M. (2007). N-cadherin mediates cortical organization in the mouse brain. *Dev Biol* **304**, 22-33.

Kanner, S. B., Reynolds, A. B. and Parsons, J. T. (1991). Tyrosine phosphorylation of a 120-kilodalton pp60src substrate upon epidermal growth factor and platelet-derived growth factor receptor stimulation and in polyomavirus middle-T-antigen-transformed cells. *Mol Cell Biol* **11**, 713-20.

Kashima, T., Nakamura, K., Kawaguchi, J., Takanashi, M., Ishida, T., Aburatani, H., Kudo, A., Fukayama, M. and Grigoriadis, A. E. (2003). Overexpression of cadherins suppresses pulmonary metastasis of osteosarcoma in vivo. *Int J Cancer* **104**, 147-54.

Kawauchi, T., Sekine, K., Shikanai, M., Chihama, K., Tomita, K., Kubo, K., Nakajima, K., Nabeshima, Y. and Hoshino, M. (2010). Rab GTPases-dependent endocytic pathways regulate neuronal migration and maturation through N-cadherin trafficking. *Neuron* **67**, 588-602.

Ke, Y., Wilkinson, M. C., Fernig, D. G., Smith, J. A., Rudland, P. S. and Barraclough, R. (1992). A rapid procedure for production of human basic fibroblast growth factor in Escherichia coli cells. *Biochim Biophys Acta* **1131**, 307-10.

Kolijn, K., Verhoef, E. I. and van Leenders, G. J. (2015). Morphological and immunohistochemical identification of epithelial-to-mesenchymal transition in clinical prostate cancer. *Oncotarget* **6**, 24488-98.

Kontaridis, M. I., Liu, X., Zhang, L. and Bennett, A. M. (2002). Role of SHP-2 in fibroblast growth factor receptor-mediated suppression of myogenesis in C2C12 myoblasts. *Mol Cell Biol* **22**, 3875-91.

Kourtidis, A., Yanagisawa, M., Huveldt, D., Copland, J. A. and Anastasiadis, P. Z. (2015). Pro-Tumorigenic Phosphorylation of p120 Catenin in Renal and Breast Cancer. *PLoS One* **10**, e0129964.

Lambert, M., Thoumine, O., Brevier, J., Choquet, D., Riveline, D. and Mege, R. M. (2007). Nucleation and growth of cadherin adhesions. *Exp Cell Res* **313**, 4025-4040.

Lebreton, G. and Casanova, J. (2016). Ligand-binding and constitutive FGF receptors in single Drosophila tracheal cells: Implications for the role of FGF in collective migration. *Dev Dyn* **245**, 372-8.

Lemmon, M. A. and Schlessinger, J. (2010). Cell signaling by receptor tyrosine kinases. *Cell* **141**, 1117-34.

Letourneau, P. C., Shattuck, T. A., Roche, F. K., Takeichi, M. and Lemmon, V. (1990). Nerve growth cone migration onto Schwann cells involves the calcium-dependent adhesion molecule, N-cadherin. *Dev Biol* **138**, 430-42.

Li, G., Satyamoorthy, K. and Herlyn, M. (2001). N-cadherin-mediated intercellular interactions promote survival and migration of melanoma cells. *Cancer Res* **61**, 3819-25.

Luccardini, C., Hennekinne, L., Viou, L., Yanagida, M., Murakami, F., Kessaris, N., Ma, X., Adelstein, R. S., Mege, R. M. and Metin, C. (2013). N-cadherin sustains motility and polarity of future cortical interneurons during tangential migration. *J Neurosci* **33**, 18149-60.

Mariner, D. J., Anastasiadis, P., Keilhack, H., Bohmer, F. D., Wang, J. and Reynolds, A. B. (2001). Identification of Src phosphorylation sites in the catenin p120ctn. *J Biol Chem* **276**, 28006-13.

Matsunaga, M., Hatta, K., Nagafuchi, A. and Takeichi, M. (1988). Guidance of optic nerve fibres by N-cadherin adhesion molecules. *Nature* **334**, 62-4.

bioRxiv preprint doi: https://doi.org/10.1101/465930; this version posted November 8, 2018. The copyright holder for this preprint (which was not certified by peer review) is the author/funder. All rights reserved. No reuse allowed without permission.

Mayor, R. and Etienne-Manneville, S. (2016). The front and rear of collective cell migration. *Nat Rev Mol Cell Biol* **17**, 97-109.

McCrea, P. D., Maher, M. T. and Gottardi, C. J. (2015). Nuclear signaling from cadherin adhesion complexes. *Curr Top Dev Biol* **112**, 129-96.

McIntosh, I., Bellus, G. A. and Jab, E. W. (2000). The pleiotropic effects of fibroblast growth factor receptors in mammalian development. *Cell Struct Funct* **25**, 85-96.

Mege, R. M. and Ishiyama, N. (2017). Integration of Cadherin Adhesion and Cytoskeleton at Adherens Junctions. *Cold Spring Harb Perspect Biol*.

Meng, W. and Takeichi, M. (2009). Adherens junction: molecular architecture and regulation. *Cold Spring Harb Perspect Biol* **1**, a002899.

Nagi, C., Guttman, M., Jaffer, S., Qiao, R., Keren, R., Triana, A., Li, M., Godbold, J., Bleiweiss, I. J. and Hazan, R. B. (2005). N-cadherin expression in breast cancer: correlation with an aggressive histologic variant--invasive micropapillary carcinoma. *Breast Cancer Res Treat* **94**, 225-35.

Nakashima, T., Huang, C., Liu, D., Kameyama, K., Masuya, D., Kobayashi, S., Kinoshita, M. and Yokomise, H. (2003). Neural-cadherin expression associated with angiogenesis in non-small-cell lung cancer patients. *Br J Cancer* **88**, 1727-33.

Nguyen, T. and Mege, R. M. (2016). N-Cadherin and Fibroblast Growth Factor Receptors crosstalk in the control of developmental and cancer cell migrations. *Eur J Cell Biol* **95**, 415-426.

Palecek, S. P., Loftus, J. C., Ginsberg, M. H., Lauffenburger, D. A. and Horwitz, A. F. (1997). Integrin-ligand binding properties govern cell migration speed through cell-substratum adhesiveness. *Nature* **385**, 537-40.

Peterson, S. J. and Krasnow, M. A. (2015). Subcellular trafficking of FGF controls tracheal invasion of Drosophila flight muscle. *Cell* **160**, 313-23.

Peyton, S. R. and Putnam, A. J. (2005). Extracellular matrix rigidity governs smooth muscle cell motility in a biphasic fashion. *J Cell Physiol* **204**, 198-209.

Plestant, C., Strale, P. O., Seddiki, R., Nguyen, E., Ladoux, B. and Mege, R. M. (2014). Adhesive interactions of N-cadherin limit the recruitment of microtubules to cell-cell contacts through organization of actomyosin. *J Cell Sci* **127**, 1660-71.

Porta, R., Borea, R., Coelho, A., Khan, S., Araujo, A., Reclusa, P., Franchina, T., Van Der Steen, N., Van Dam, P., Ferri, J. et al. (2017). FGFR a promising druggable target in cancer: Molecular biology and new drugs. *Crit Rev Oncol Hematol* **113**, 256-267.

Prasad, M., Wang, X., He, L. and Montell, D. J. (2011). Border cell migration: a model system for live imaging and genetic analysis of collective cell movement. *Methods Mol Biol* **769**, 277-86.

Redies, C. and Takeichi, M. (1996). Cadherins in the developing central nervous system: an adhesive code for segmental and functional subdivisions. *Dev Biol* **180**, 413-23.

Ren, M., Qin, H., Ren, R., Tidwell, J. and Cowell, J. K. (2011). Src activation plays an important key role in lymphomagenesis induced by FGFR1 fusion kinases. *Cancer Res* **71**, 7312-22.

Rieger-Christ, K. M., Lee, P., Zagha, R., Kosakowski, M., Moinzadeh, A., Stoffel, J., Ben-Ze'ev, A., Libertino, J. A. and Summerhayes, I. C. (2004). Novel expression of N-cadherin elicits in vitro bladder cell invasion via the Akt signaling pathway. *Oncogene* **23**, 4745-53.

Scarpa, E., Szabo, A., Bibonne, A., Theveneau, E., Parsons, M. and Mayor, R. (2015). Cadherin Switch during EMT in Neural Crest Cells Leads to Contact Inhibition of Locomotion via Repolarization of Forces. *Dev Cell* **34**, 421-34.

Strale, P. O., Duchesne, L., Peyret, G., Montel, L., Nguyen, T., Png, E., Tampe, R., Troyanovsky, S., Henon, S., Ladoux, B. et al. (2015). The formation of ordered nanoclusters controls cadherin anchoring to actin and cell-cell contact fluidity. *J Cell Biol* **210**, 333-46.

Suyama, K., Shapiro, I., Guttman, M. and Hazan, R. B. (2002). A signaling pathway leading to metastasis is controlled by N-cadherin and the FGF receptor. *Cancer Cell* **2**, 301-14.

Suzuki, S. C. and Takeichi, M. (2008). Cadherins in neuronal morphogenesis and function. *Dev Growth Differ* **50 Suppl 1**, S119-30.

Taeger, J., Moser, C., Hellerbrand, C., Mycielska, M. E., Glockzin, G., Schlitt, H. J., Geissler, E. K., Stoeltzing, O. and Lang, S. A. (2011). Targeting FGFR/PDGFR/VEGFR impairs tumor growth,

bioRxiv preprint doi: https://doi.org/10.1101/465930; this version posted November 8, 2018. The copyright holder for this preprint (which was not certified by peer review) is the author/funder. All rights reserved. No reuse allowed without permission.

angiogenesis, and metastasis by effects on tumor cells, endothelial cells, and pericytes in pancreatic cancer. *Mol Cancer Ther* **10**, 2157-67.

Takehara, T., Teramura, T., Onodera, Y., Frampton, J. and Fukuda, K. (2015). Cdh2 stabilizes FGFR1 and contributes to primed-state pluripotency in mouse epiblast stem cells. *Sci Rep* **5**, 14722.

Thoreson, M. A., Anastasiadis, P. Z., Daniel, J. M., Ireton, R. C., Wheelock, M. J., Johnson, K. R., Hummingbird, D. K. and Reynolds, A. B. (2000). Selective uncoupling of p120(ctn) from E-cadherin disrupts strong adhesion. *J Cell Biol* **148**, 189-202.

Thoumine, O., Lambert, M., Mege, R. M. and Choquet, D. (2006). Regulation of N-cadherin dynamics at neuronal contacts by ligand binding and cytoskeletal coupling. *Mol Biol Cell* **17**, 862-75.

Treubert-Zimmermann, U., Heyers, D. and Redies, C. (2002). Targeting axons to specific fiber tracts in vivo by altering cadherin expression. *J Neurosci* **22**, 7617-26.

Trolice, M. P., Pappalardo, A. and Peluso, J. J. (1997). Basic fibroblast growth factor and N-cadherin maintain rat granulosa cell and ovarian surface epithelial cell viability by stimulating the tyrosine phosphorylation of the fibroblast growth factor receptors. *Endocrinology* **138**, 107-13.

Utton, M. A., Eickholt, B., Howell, F. V., Wallis, J. and Doherty, P. (2001). Soluble N-cadherin stimulates fibroblast growth factor receptor dependent neurite outgrowth and N-cadherin and the fibroblast growth factor receptor co-cluster in cells. *J Neurochem* **76**, 1421-30.

van Roy, F. (2014). Beyond E-cadherin: roles of other cadherin superfamily members in cancer. *Nat Rev Cancer* **14**, 121-34.

van Roy, F. and Berx, G. (2008). The cell-cell adhesion molecule E-cadherin. *Cell Mol Life Sci* **65**, 3756-88.

Vedula, S. R., Ravasio, A., Anon, E., Chen, T., Peyret, G., Ashraf, M. and Ladoux, B. (2014). Microfabricated environments to study collective cell behaviors. *Methods Cell Biol* **120**, 235-52.

Wesche, J., Haglund, K. and Haugsten, E. M. (2011). Fibroblast growth factors and their receptors in cancer. *Biochem J* **437**, 199-213.

Wheelock, M. J., Soler, A. P. and Knudsen, K. A. (2001). Cadherin junctions in mammary tumors. *J Mammary Gland Biol Neoplasia* **6**, 275-85.

Williams, E. J., Furness, J., Walsh, F. S. and Doherty, P. (1994). Activation of the FGF receptor underlies neurite outgrowth stimulated by L1, N-CAM, and N-cadherin. *Neuron* **13**, 583-94.

Yamaguchi, T. P., Harpal, K., Henkemeyer, M. and Rossant, J. (1994). fgfr-1 is required for embryonic growth and mesodermal patterning during mouse gastrulation. *Genes Dev* **8**, 3032-44.

Zhan, X., Plourde, C., Hu, X., Friesel, R. and Maciag, T. (1994). Association of fibroblast growth factor receptor-1 with c-Src correlates with association between c-Src and cortactin. *J Biol Chem* **269**, 20221-4.

bioRxiv preprint doi: https://doi.org/10.1101/465930; this version posted November 8, 2018. The copyright holder for this preprint (which was not certified by peer review) is the author/funder. All rights reserved. No reuse allowed without permission.

Figure Legends

Figure 1: FGFR decreases the migration of N-cadherin expressing cells on N-cadherin coated lines. DsRed-Ncad (Ncad) and DsRed-Ncad/GFP-FGFR (Ncad/FGFR) expressing HEK cells were seeded at low density on 10 µm-width Ncad-Fc coated lines in the absence or in the presence of FGFR inhibitor (Ncad/FGFR+inh) and imaged in phase contrast every 6 minutes during 20 hours (see Video 1). **(A)** Representative kymographs of the displacement over 10 hours of two cells for each condition. **(B)** Tracked displacements over 20 hours of Ncad (n = 26), Ncad/FGFR (n= 22) and Ncad/FGFR+inh (n = 25) cells. **(C)** Representative kymographs of 1-hour long cell displacements imaged at higher magnification (see Video 1). **(D, E)** Histograms representing the mean cell body speed and the frequency of inversion in migration direction, respectively, for Ncad, Ncad/FGFR and Ncad/FGFR+inh cells (** $p \leq 0.01$, *** $p \leq 0.0001$, ANOVA multi-comparison test, Newman-Keuls post-test). **(F)** Plots of the mean cell body speed as a function of cell surface area for the three cell populations.

Figure 2: FGFR and N-cadherin co-stabilize each other at cell-cell contacts. (A) Representative images of FRAP experiments performed at the cell-cell contacts of DsRed-Ncad HEK cells: Fluorescent signal before (Pre-bleach), immediately after bleaching (Bleach) and 110 sec after the bleach (Post-bleach). Red rectangles represent the bleached region at cell-cell contacts. Scale bar: 40 µm. **(B)** Left: normalized DsRed-Ncad fluorescence recovery curves for Ncad, Ncad/FGFR and Ncad/FGFR+inh cells, respectively. $n \geq 20$. Right: mean Ncad mobile fraction ± SEM, *** $p \leq 0.001$; ns: non-significant, ANOVA multiple comparison test, $n \geq 20$). **(C)** Left: normalized fluorescence recovery for GFP-FGFR in FGFR, FGFR/Ecad and FGFR/ Ncad cells, respectively. n =15. Right: mean FGFR mobile fraction ± SEM), *** $p \leq 0.0001$; ns: non-significant, ANOVA multi-comparison test, ($n \geq 14$). **(D)** Left: normalized mCherry-Ecad fluorescence recovery in mCherry-Ecad (grey) and mCherry-Ecad/FGFR (black) cells, respectively. $n \geq 20$, Right: mean mCherry-Ecad mobile fraction ± SEM, ns: non-significant, student t-test, n = 18.

Figure 3: FGFR1 expression promotes N-cadherin recruitment and strengthens cell-cell contacts. (A) DsRed-Ncad distribution in fixed monolayers of Ncad, Ncad/FGFR cells and Ncad/FGFR+inh cells grown overnight on glass coverslips in the presence of serum

bioRxiv preprint doi: https://doi.org/10.1101/465930; this version posted November 8, 2018. The copyright holder for this preprint (which was not certified by peer review) is the author/funder. All rights reserved. No reuse allowed without permission.

(fibronectin/vitronectin coating). Scale bar: 20 µm. Boxes show zoomed views of cell-cell contacts indicated by arrows. Cell-cell contacts in Ncad/FGFR cells appear straighter than those in Ncad cells and Ncad/FGFR+inh cells. Histograms on the right show DsRed-Ncad intensities measured at the cell-cell contacts in the three conditions thanks to Imaris. *** $p \leq 0.0001$; ** $p < 0.01$; ns: non-significant, ANOVA multi-comparison test, ($n \geq 50$). **(B)** Ncad and Ncad/FGFR cells were seeded on 10 µm width fibronectin-coated stripes and fixed after 2 hours. Left: cell doublets were imaged (scale bar: 20 µm). Right: the graphs show the mean distribution of DeRed-N-cad intensity along the cell width (z axis) normalized along the x axis of the cell with 0 value defined as the junctional edge of the cell and 1 value as the free edge, for Ncad and Ncad/FGFR cells (n = 30 and 27 doublets, respectively, SD = 0.177)). **(C)** Analysis by flow cytometry imaging of Ncad recruitment at cell-cell interface in cell doublets. DsRed-Ncad recruitment at cell-cell contacts was quantified as the average normalized Ncad fluorescence intensity per surface unit in cell-cell areas (Ncad int./S.U.). FGFR expression significantly increased Ncad recruitment at cell-cell contacts. Bright detail intensities analysis (BDI) was applied to quantify fluorescence heterogeneity in cell-cell contact regions. Ncad fluorescence foci formation per surface unit (Ncad BDI/ U.I.) was increased in Ncad/FGFR cells compared to Ncad cells. n = 4 populations of 150.000 cells.

Figure 4: FGFR strengthens N-cadherin-mediated cell-cell contacts and reinforces N-cadherin anchoring to the cell cortex. (A-C) Ncad, Ncad/FGFR, Ncad/FGFR + inh cells cultured at confluence over 1 mm^2 square fibronectin-coated-patterns were treated with EGTA then imaged for DsRed-Ncad every 30 seconds during 15 min. **(A)** Low magnification images taken after 5 min of EGTA treatment. Scale bar = 40 µm. **(B)** Examples of kymographs of the DsRed-Ncad signal along a line perpendicular to the cell-cell contact starting from EGTA addition (t_0) for Ncad, Ncad/FGFR and Ncad/FGFR+inh cells. **(C)** Contact dissociation time upon EGTA addition as determined from the kymographs for the three conditions. ** $p \leq 0.01$; *** $p \leq 0.001$, ANOVA multi comparison test, Newman-Keuls post-test, n = 60 contacts. **(D)** Left: magnetic tweezers experimental set up used to evaluate the anchorage and rupture force of N-cadherin mediated bead-cell contacts. Right: Calibration curve of the magnetic tweezers determined as described in material and methods. The force is exponentially anti-correlated with the bead-magnetic needle distance. **(E)** Representative images of Ncad-coated beads before and after tweezer-induced detachment from the cell membrane. **(F)** Distribution of the responses of Ncad beads to the magnetic field in three

bioRxiv preprint doi: https://doi.org/10.1101/465930; this version posted November 8, 2018. The copyright holder for this preprint (which was not certified by peer review) is the author/funder. All rights reserved. No reuse allowed without permission.

classes (release, displacement, and immobility) for Ncad (n=60), Ncad/FGFR (n=65) and Ncad/FGFR+inh (n=50) cells. **(G)** Bead-cell contact disruption forces calculated from the Stoke equation for Ncad, Ncad/FGFR and Ncad/FGFR + inh HEK cells (*** $p \leq 0.001$, ANOVA multi comparison test, Newman-Keuls post-test).

Figure 5: N-cadherin and FGFR associate leading to increased activation of FGFR. (A) Binding of Ncad-Fc to FGFR1 extracellular domain. Kinetics of Ncad-Fc to immobilized FGFR1 extracellular domain was measured as described under "Materials and Methods." Left panel: Ncad-Fc at different concentrations was added to a FGFR1-derivatized cuvette and the association reaction was followed for 200 s. Data were collected three times a second. The concentration of Ncad-Fc is indicated. Data shown are the result of one representative experiment out of three. Right panel: relationship between the extent of binding (response in arc s) of the association reactions shown in left and Ncad-Fc concentration. All results are summarized in table 1. **(B)** GFP-FGFR was immunoprecipitated with anti-GFP bead from protein extracts of Ncad, FGFR and Ncad/FGFR cells. Immunoprecipitates, together with total protein extracts, were then analyzed by Western blot using anti-Ncad and anti-GFP (FGFR) antibodies. The histogram shows the ratio of N-cadherin bound to GFP-FGFR on N-cadherin in total extract, determined from the quantification of 3 independent immunoblots then converted to percentage. ** $p \leq 0.01$, Student's t test, n=3. **(C)** To detect FGFR phosphorylation GFP-FGFR immuno-precipitates were immunoblotted with anti-P-Tyr and anti-GFP (FGFR) antibodies. The histogram shows the ratio of P-Tyr on GFP-FGFR signals as a quantification of the degree of phosphorylation of FGFR in the different extracts. ** $p \leq 0.01$, Student's *t* test, n=3.

Figure 6: FGFR increases N-cadherin cell surface accumulation by reducing its endocytosis. (A) Analysis of cell surface expression of N-cadherin. Left: cell surface protein biotinylation; Cy5-conjugated streptavidin labelling of freshly biotinylated cells and of biotinylated cells following reducing wash. Right: After surface biotinylation at cold and removal of unfixed biotin, Ncad, Ncad/FGFR and Ncad/FGFR+inh cells were immediately lysed and protein extracts subjected to precipitation by streptavidin beads. GFP transfected HEK cells were used as control. Total extracts and streptavidin bound fractions (plasma membrane exposed fractions) were then immunoblotted with anti-N-cadherin antibodies. The

bioRxiv preprint doi: https://doi.org/10.1101/465930; this version posted November 8, 2018. The copyright holder for this preprint (which was not certified by peer review) is the author/funder. All rights reserved. No reuse allowed without permission.

histogram shows the quantification of N-cadherin exposed at the plasma membrane over total N-cadherin content for the three conditions (n and statistics?). **(B)** Analysis of Ncad internal pool by flow cytometry imaging. Ncad and Ncad/FGFR cells were non-enzymatically detached, then processed for flow cytometry imaging in bright field, and for dsRed-Ncad and GFP-FGFR fluorescence imaging. Masks were defined on bright field images to separate cell membrane and internal cell areas on each cell. Applied to the fluorescence images they allowed to extract an internalization score as described in Materials & Methods. FGFR reduces the internalization score of N-cadherin molecule by 17% (1.09 U.I versus 1.32 U.I). Experiences were repeated 4 times, over populations of 150.000 cells for each condition in each experiment. **(C)** Ncad and Ncad/FGFR cells were seeded on Ncad-coated stripes of 10 µm, then after4 hours, preparations were imaged at 63X for Ds-Red Ncad. The panels show the maximum projection of 1µm thick confocal sections encompassing the whole cell thickness. Arrow-heads show N-cadherin puncta trafficking from the leading edge to the rear of Ncad expressing cells. The histogram shows the quantification of the percentage of cells with such puncta. **$p \leq 0.01$; non parametrical t test; n = 15, n = 20 cells for Ncad and Ncad/FGFR cells, respectively. **(D)** Analysis of N-cad endocytic fraction following cell surface biotinylation. Freshly biotinylated Ncad and Ncad/FGFR cells were switched to 37°C for 40 minutes to allow endocytosis to resume in the presence or in the absence of dynasore, then subject to a reducing wash in order to remove remaining medium exposed biotin. Left: cells were lysed and protein extracts subjected to precipitation by streptavidin beads, then anti-N-cadherin bound (total) and streptavidin bound fractions (endocytosed) were immunoblotted with anti-N-cadherin antibodies. Right: The hisrogram shows the ratio of endocytosed over total Ncad in each extract. *** $p \leq 0.001$; ns: non-significant, ANOVA multiple comparison test, n = 3 experiments.

Figure 7: p120 is involved in the stabilization of N-cadherin at cell-cell contacts and the decreased migration induced by FGFR expression. **(A)** Ncad and Ncad/Flag-FGFR cells were transfected with GFP-p120 and seeded on fibronectin coated lines. Mean p120 intensities along the cell length with 0 as junctional end and 1 as free end of the cell was calculated on 25 cell doublets. p120 junctional accumulation was higher in Ncad/FGFR cell doublets than in Ncad doublets. **(B)** FRAP experiments were performed on cells expressing GFP-FGFR1 and either DsRed-Ncad or mCherry-NcadAAA. Curves show Ncad and NcadAAA normalized fluorescence recoveries over time for Ncad/FGFR (black) and

bioRxiv preprint doi: https://doi.org/10.1101/465930; this version posted November 8, 2018. The copyright holder for this preprint (which was not certified by peer review) is the author/funder. All rights reserved. No reuse allowed without permission.

NcadAAA-FGFR (red) cells (mobile fraction 0.29 ± 0.1 and 0.50 ± 0.1, respectively (n ≥ 20), (***, p ≤ 0.0001, Mann-Whitney t test). **(C)** Ncad/FGFR and NcadAAA/FGFR cells were seeded on Ncad-Fc coated stripes and imaged every 6 minutes during 20 hours. Left: examples of Ncad/FGFR and NcadAAA/FGFR individual cell displacements over 1 hour. Right: histograms representing the mean cell speeds as a function of cell areas. **(D)** Plots show the displacement in function of time for Ncad/FGFR (left), NcadAAA/FGFR (right) cells with respectively n =30, n= 40 cells. Histograms show the mean speed of Ncad/FGFR (black), NcadAAA/FGFR (red) cells (****, p ≤ 0.0001, ANOVA multi-comparison test).

Figure 8: Src activity is involved in the stabilization of N-cadherin at cell-cell contacts and the decreased migration induced by FGFR expression. (A) Western blot detection of N-cad, Src and phosphorylated Src (P-Src) in the Ncad immunoprecipitates. Histogram shows the ratio of phosphorylated Src calculated as the ratio of P-Src band's intensity on Src band's intensity. **(B)** FRAP experiments were performed on DsRd-N-cadherin at cell-cell contacts of Ncad and Ncad/FGFR in the absence or in the presence of Src inhibitor. Curves and histograms show Ncad and NcadAAA normalized fluorescence recoveries over time and extracted mobile fractions ± SEM, *** p ≤ 0.001; ns: non-significant, ANOVA multiple comparison test, n =18). **(C)** Migration of Ncad/FGFR and Ncad/FGFR cells treated with the Src inhibitor on Ncad-Fc coated lines. Graph shows the cumulative cell displacements in function of time and histogram the mean cell migration speeds. (** p≤ 0,01, *** p ≤ 0.0001, ANOVA multi-comparison test, Newman-Keuls post-test).

Figure 9: FGFR promotes N-cadherin-F-actin functional mechanocoupling. (A) LifeAct-GFP expressing C2C12 cells were seeded on Ncad-Fc coated surfaces for 2 hours, than treated with or without FGFR inhibitor for 1 hour, and then imaged for 5 minutes at a frequency of two images per second. Left: still images of the LifeAct-GFP signal, scale bar = 20 µm. Inserts on the right represent examples of kymograph constructed along the two pixel-wide yellow lines (1–3), Right: the actin retrograde flow was quantified by kymograph analysis. Right:the histogram shows the mean actin retrograde flow speed for C2C12 (n = 140 kymographs from 24 cells) and C2C12 + inh (n = 156 kymographs from 25 cells) cells, (**** p ≤ 0.0002, Student's *t* test). **(B)** Migration on Ncad-Fc coated lines of Ncad and Ncad/FGFR cells treated with the Arp2/3 inhibitor. Left: kymographs of the displacement over 10 hours of

bioRxiv preprint doi: https://doi.org/10.1101/465930; this version posted November 8, 2018. The copyright holder for this preprint (which was not certified by peer review) is the author/funder. All rights reserved. No reuse allowed without permission.

three cells for each condition. Middle: cumulative displacements of cells in function of time (20 hours) for Ncad + CK666 (n = 26), Ncad/ FGFR + CK666 (n= 22) cells. . Right: histograms representing the mean cell speed for each condition (** $p \leq 0,01$, *** $p \leq 0.0001$, ANOVA multi-comparison test, Newman-Keuls post-test).

bioRxiv preprint doi: https://doi.org/10.1101/465930; this version posted November 8, 2018. The copyright holder for this preprint (which was not certified by peer review) is the author/funder. All rights reserved. No reuse allowed without permission.

Supplemental Figure Legends

Figure S1: FGFR enhances the recruitment and the clustering of N-cadherin at cell-cell contacts. (A) Distribution plot of values obtained for the normalized Ncad fluorescence intensity per surface unit at cell-cell areas (Ncad int./S.U.) presented in Figure 3C. **(B)** Distribution plot of values obtained for bright detail intensities analysis (BDI) at cell-cell areas (Ncad BDI/S.U.) presented in Figure 3C

Figure S2: Enhanced N-cadherin engagement sustains activation of FGFR downstream pathway. C2C12 cells expressing endogenous N-cadherin were treated with FGF2 (5 nM, 15 minutes) or/and with FGFR inhibitor (10 nM, 1 hour) **(A);** or preincubated with EGTA (2mM, 30 minutes), then switch back to medium containing 2 mM Ca2+ for 10 minutes in the absence or in the presence of FGFR inhibitor **(B).** Cells were lysed and total extractions were subjected to electrophoresis and Western blotting using anti-Erk1/2 and anti-P-Erk1/2 antibodies.

Figure S3 FGFR activity decreases N-cadherin internalization. Analysis of N-cad endocytic fraction following cell surface biotinylation for Ncad, Ncad/FGFR and Ncad/FGFR + inh cells. Experiments were performed similarly than in Figure 6B except that the dynasore treatment was replaced by FGFR inhibitor treatment. (Left) Western blot detection of N-cad in anti-N-cadherin (total) and streptavidin pooled (endocytosed) proteins. (Right) Quantification of the N-cad endocytosed/total ratio obtained over 3 independent western blots. **$p \leq 0.01$; *** $p \leq 0.001$; ns: non-significant, ANOVA multiple comparison test.

Figure S4: FGFR expression reduces the total amount and cytosolic fraction of N-cadherin and p120. (A) FGFR, Ncad and Ncad/FGFR HEK cells were collected without detergent. Then total, cytosolic and membranous fractions were then separated as detailed in Material and Methods, the proteins extracted and immunoblotted. Histograms present the quantification of total level of p120 reported to actin and the ratio of p120 in membranous and

bioRxiv preprint doi: https://doi.org/10.1101/465930; this version posted November 8, 2018. The copyright holder for this preprint (which was not certified by peer review) is the author/funder. All rights reserved. No reuse allowed without permission.

cytosolic fractions versus total p120 cellular content. **p≤0.01; *** p≤0.001; ns: non-significant, unpaired t test, n = 3 experiments.

(B) Total protein extracts of GFP-HEK, Ncad, Ncad/FGFR and Ncad/FGFR cells treated with Src or FGFR inhibitor were separated and immublotted using anti-Pp120 and anti-p120 antibodies. Actin was used for protein loading control. The histogram shows the ratio of Pp120 over p120 in total extract, determined from the quantification of 3 independent immunoblots then converted to percentage.

(C) Cell extracts were immunoprecipitated with anti-N-cadherin antibodies then immunoblotted with antibodies against N-cadherin, p120 and P-p120. The ratio of p120 phosphorylation was evaluated as the ratio of P-p120 band's intensity on p120 band's intensity. The histogram presents the quantification over 3 independent experiments (****, p ≤ 0.0001, Anova multi-comparison test).

Figure S5: Effect of blebbistatin treatment on the migration of cells on N-cadherin lines. Tracked displacements over 20 hours of Ncad (n = 12), Ncad/FGFR cells (n= 13). Histogram represents the mean cell speed.

bioRxiv preprint doi: https://doi.org/10.1101/465930; this version posted November 8, 2018. The copyright holder for this preprint (which was not certified by peer review) is the author/funder. All rights reserved. No reuse allowed without permission.

	Mean	±	S.E.
k_{ass} ($M^{-1}.s^{-1}$)	225,365	±	49,622
k_{diss} (s^{-1})	0.024	±	0.002
K_D (nM) (kinetic)	106	±	25
K_D (nM) (equilibrium)	62	±	43

Table 1: Kinetics of N-cadherin binding to immobilized FGFR1 extracellular domain

Binding parameters were determined in an optical biosensor (see Materials & Methods). The standard error (S.E.) of the k_{ass} (association rate constant) was derived from the deviation of the data from a one site binding model, calculated by matrix inversion using the FASTFit software provided with the instrument. Three independent sets of k_{on} (each set was at least 5 measurements at different concentrations) were measured and the three resulting values for k_{ass} and their errors were combined. The k_{diss} (dissociation rate constant) is the mean ± S.E. of 10 values (2 independent sets of experiments), obtained at high concentrations of Ncad-Fc. The K_D (kinetic) was calculated from the ratio of k_{diss}/k_{ass} and its S.E. is the combined S.E. of the two kinetic parameters. The K_D (equilibrium) was calculated from the extent of binding at equilibrium and its S.E. is the combined S.E. of three independent determinations of K_D (equilibrium). k_D calculated from the kinetic parameters (K_D kinetics) is in the same range to the one calculated from the maximum extent of binding (*KD* equilibrium) indicating that these binding data are self-consistent.

bioRxiv preprint doi: https://doi.org/10.1101/465930; this version posted November 8, 2018. The copyright holder for this preprint (which was not certified by peer review) is the author/funder. All rights reserved. No reuse allowed without permission.

Video legends

Video1 (1mn55s): Ncad, Ncad/FGFR, Ncad/FGFR + FGFR inh cells migration on Ncad coated lines.

Video2 (12s): Magnetic tweezer experiments on Ncad, Ncad/FGFR, Ncad/FGFR + FGFR inh cells.

Video3 (48s): Ncad trafficking at the leading edge of Ncad, Ncad/FGFR migrating cells.

Video4 (1mn55s): Ncad/FGFR and NcadAAA/FGFR cells migration on Ncad coated lines.

Video5 (1mn55s): Ncad/FGFR and Ncad/FGFR+ Src inhibitor migration on Ncad coated lines.

Video6 (43s): Measurement of Ncad/actin mechanocoupling in C2C12 cells.

Video7 (1mn55s): Ncad/FGFR and Ncad/FGFR+ CK666 migration cells on Ncad coated lines.

bioRxiv preprint doi: https://doi.org/10.1101/465930; this version posted November 8, 2018. The copyright holder for this preprint (which was not certified by peer review) is the author/funder. All rights reserved. No reuse allowed without permission.

Figure 1

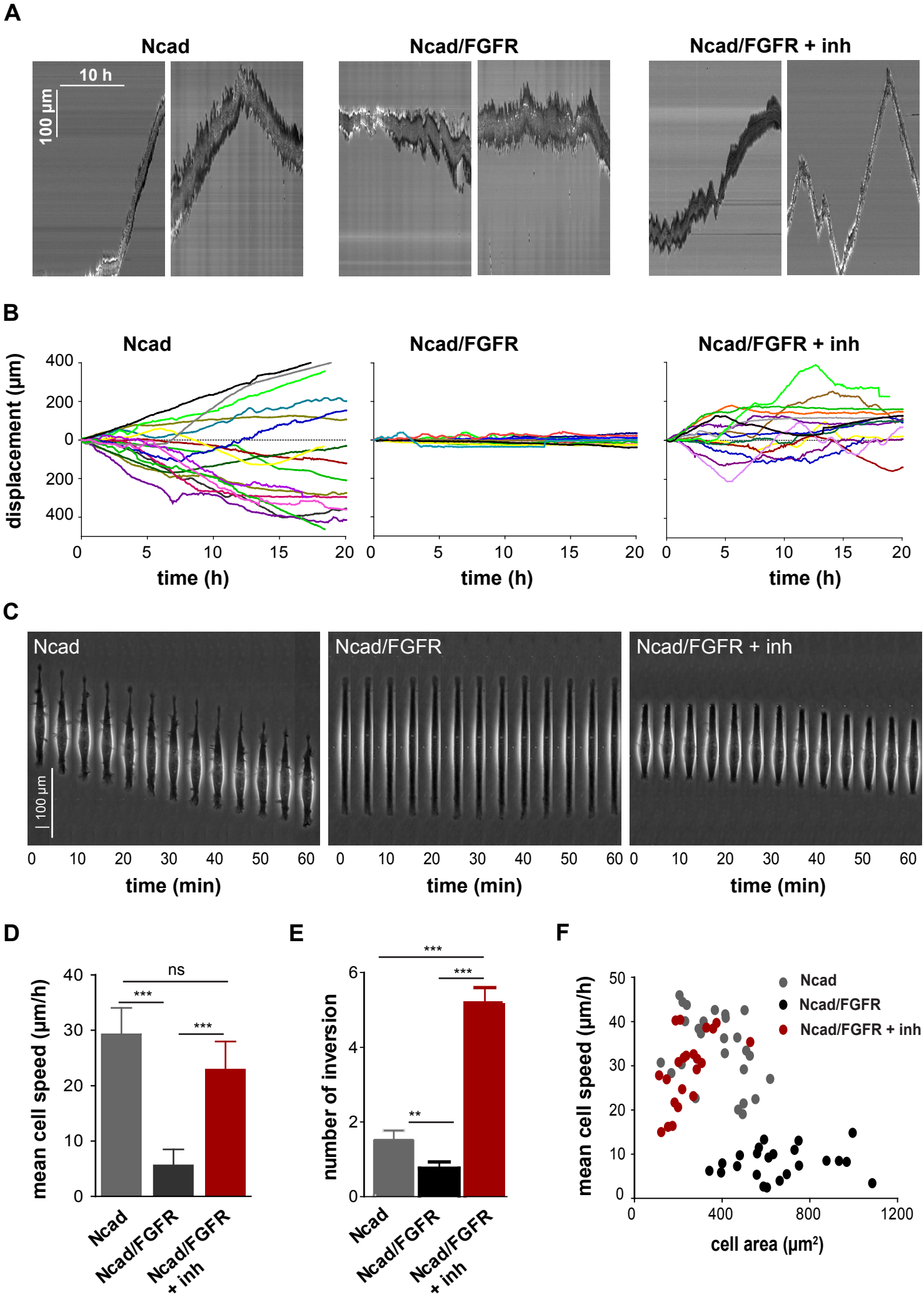

bioRxiv preprint doi: https://doi.org/10.1101/465930; this version posted November 8, 2018. The copyright holder for this preprint (which was not certified by peer review) is the author/funder. All rights reserved. No reuse allowed without permission.

Figure 2

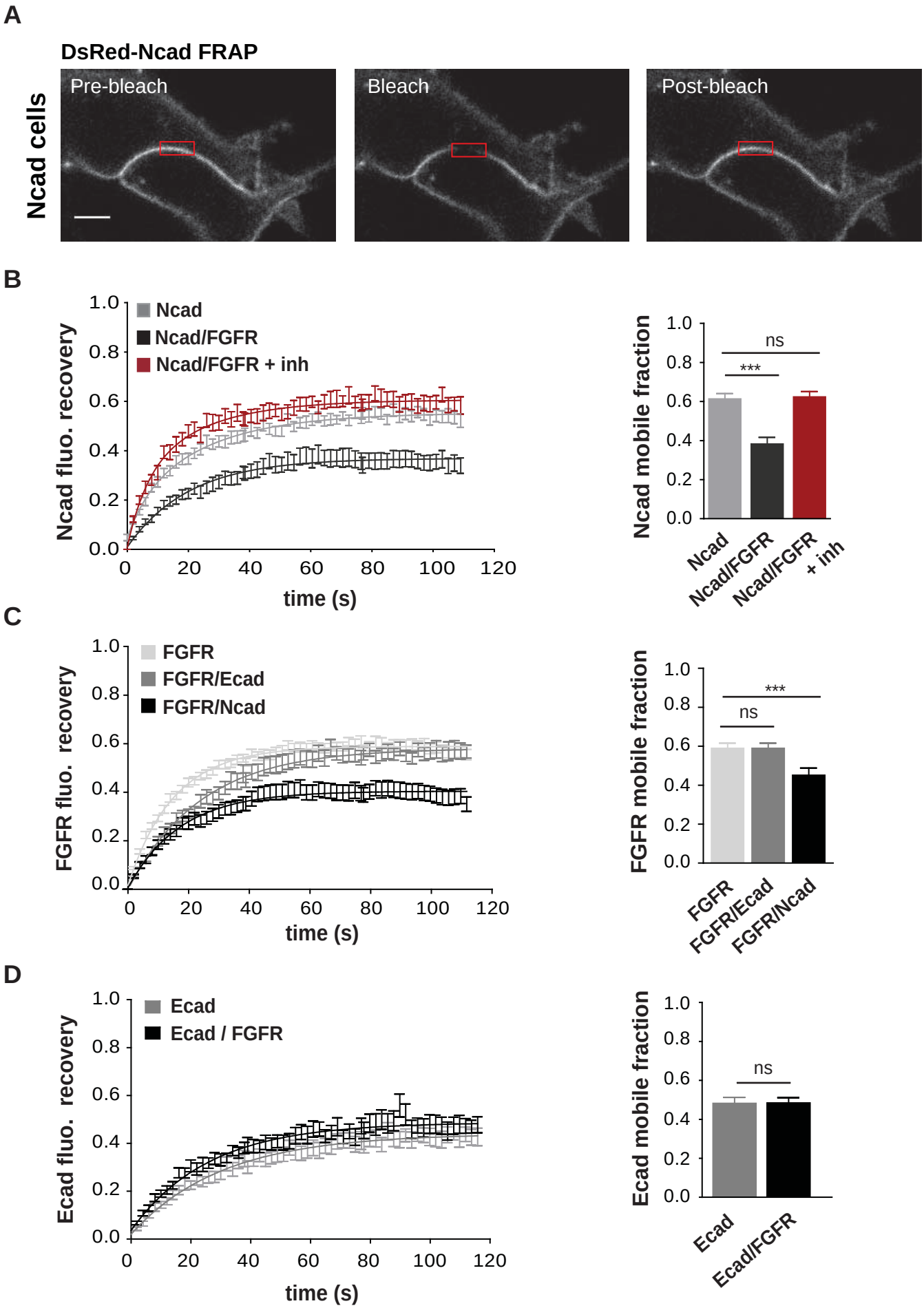

bioRxiv preprint doi: https://doi.org/10.1101/465930; this version posted November 8, 2018. The copyright holder for this preprint (which was not certified by peer review) is the author/funder. All rights reserved. No reuse allowed without permission.

Figure 3

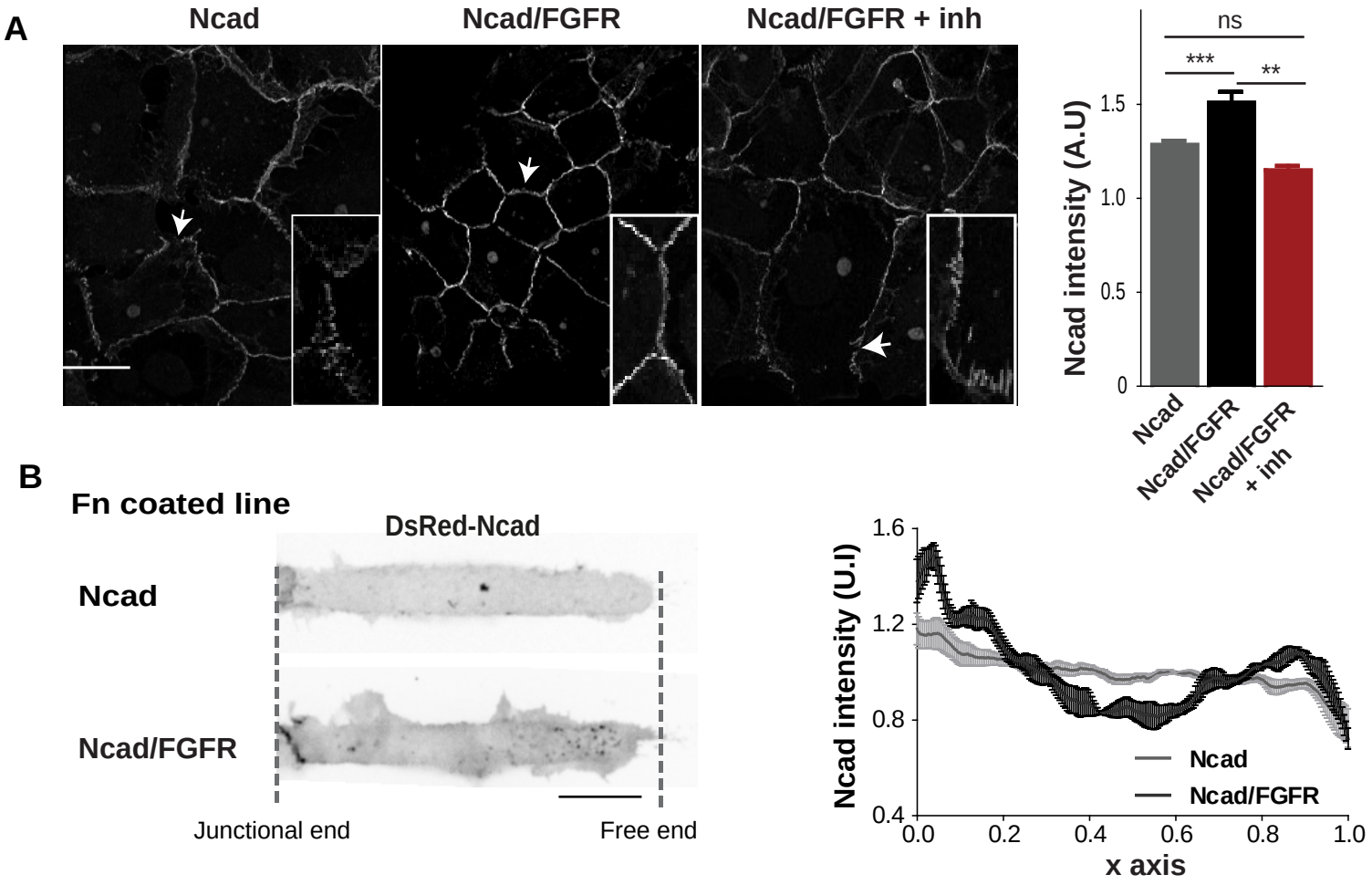

bioRxiv preprint doi: https://doi.org/10.1101/465930; this version posted November 8, 2018. The copyright holder for this preprint (which was not certified by peer review) is the author/funder. All rights reserved. No reuse allowed without permission.

Figure 4

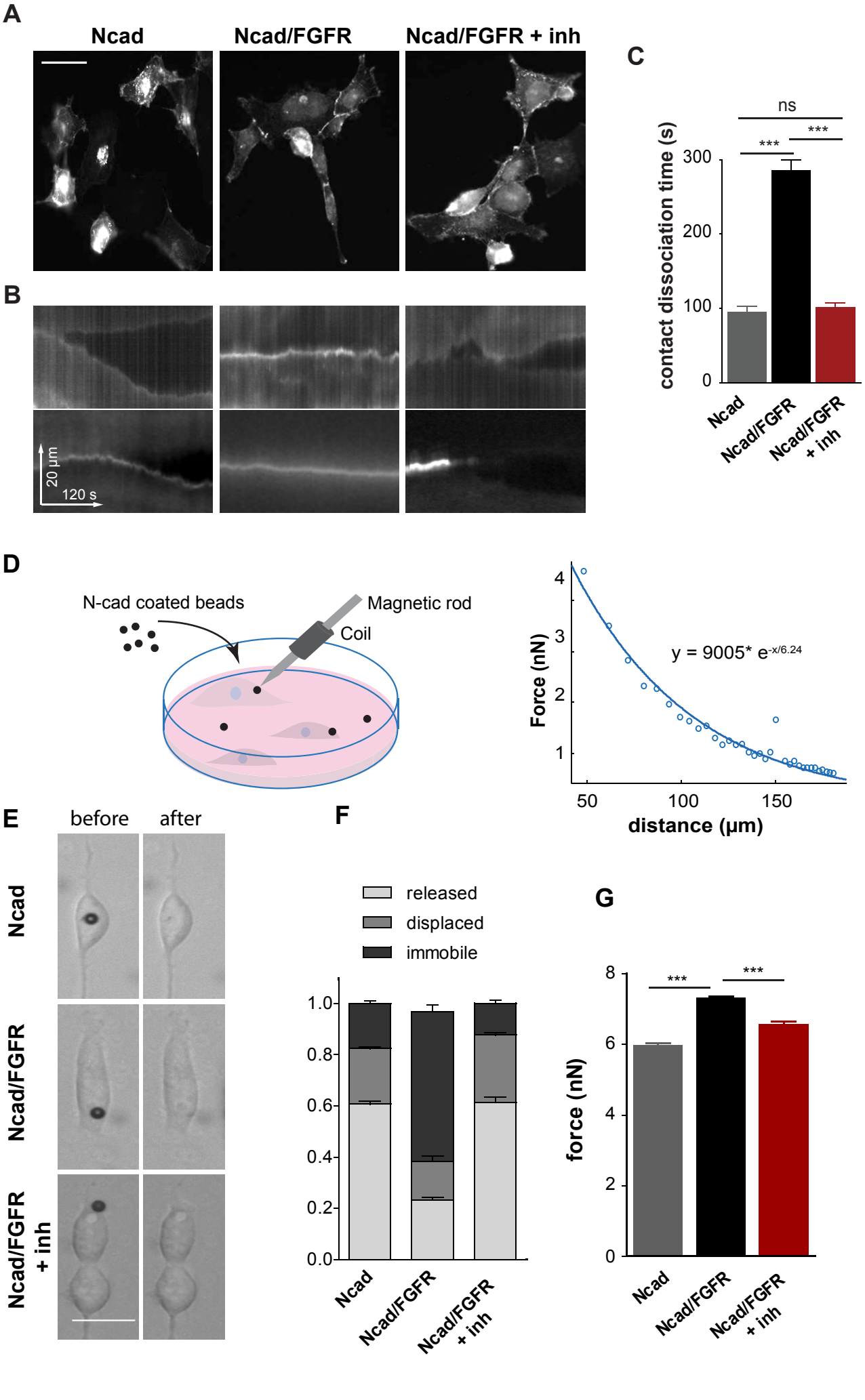

bioRxiv preprint doi: https://doi.org/10.1101/465930; this version posted November 8, 2018. The copyright holder for this preprint (which was not certified by peer review) is the author/funder. All rights reserved. No reuse allowed without permission.

Figure 5

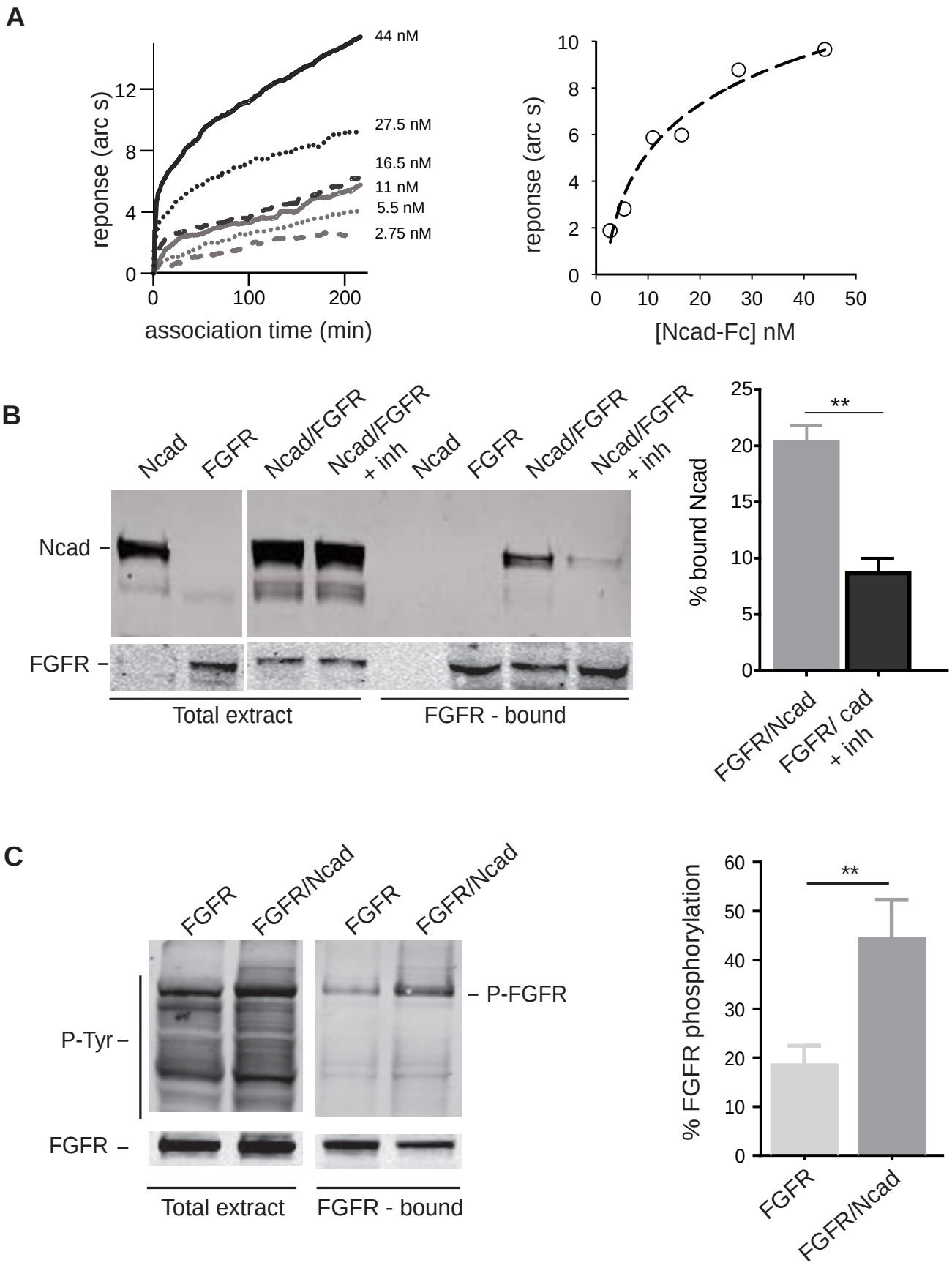

bioRxiv preprint doi: https://doi.org/10.1101/465930; this version posted November 8, 2018. The copyright holder for this preprint (which was not certified by peer review) is the author/funder. All rights reserved. No reuse allowed without permission.

Figure 6

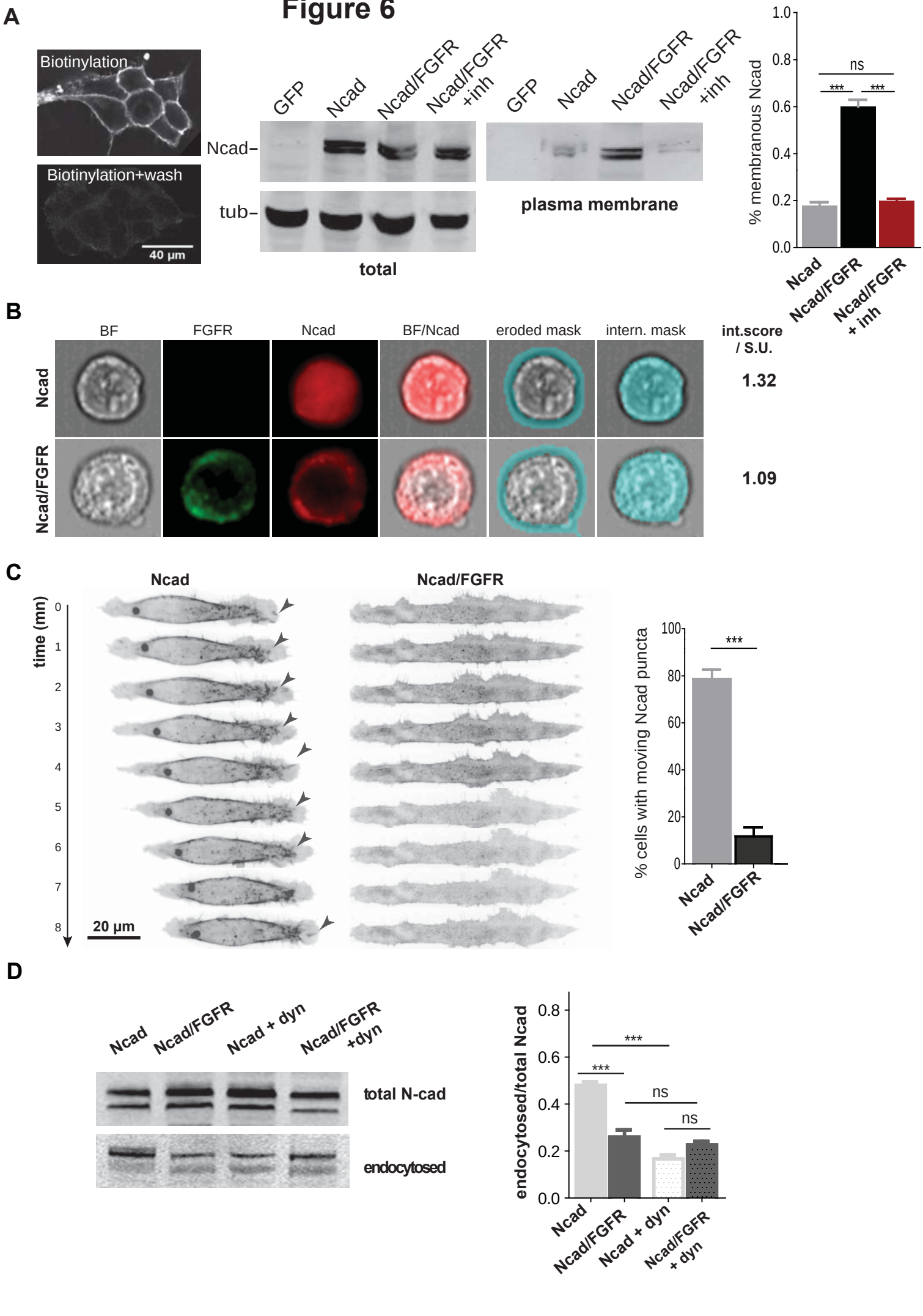

bioRxiv preprint doi: https://doi.org/10.1101/465930; this version posted November 8, 2018. The copyright holder for this preprint (which was not certified by peer review) is the author/funder. All rights reserved. No reuse allowed without permission.

Figure 7

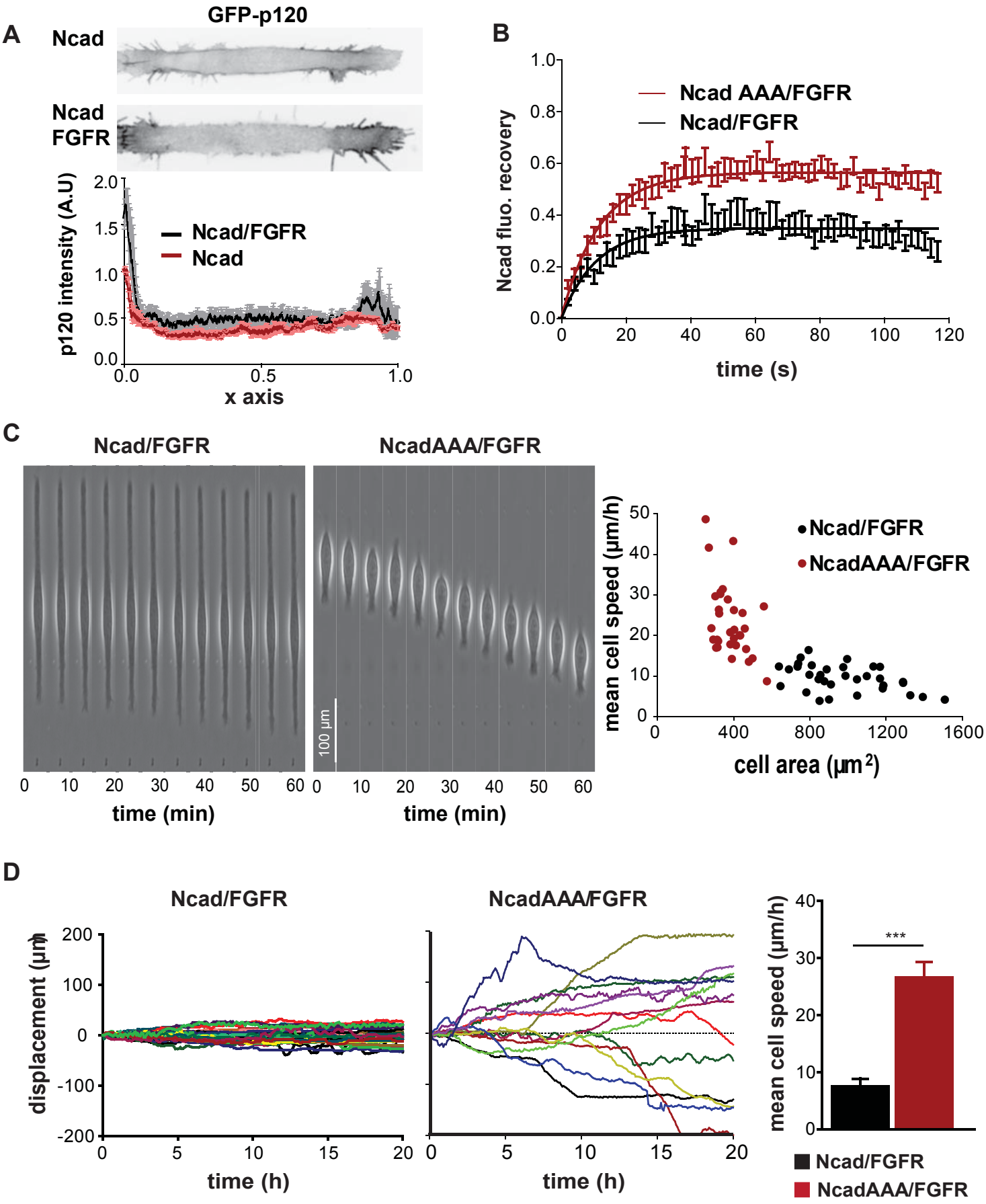

bioRxiv preprint doi: https://doi.org/10.1101/465930; this version posted November 8, 2018. The copyright holder for this preprint (which was not certified by peer review) is the author/funder. All rights reserved. No reuse allowed without permission.

Figure 8

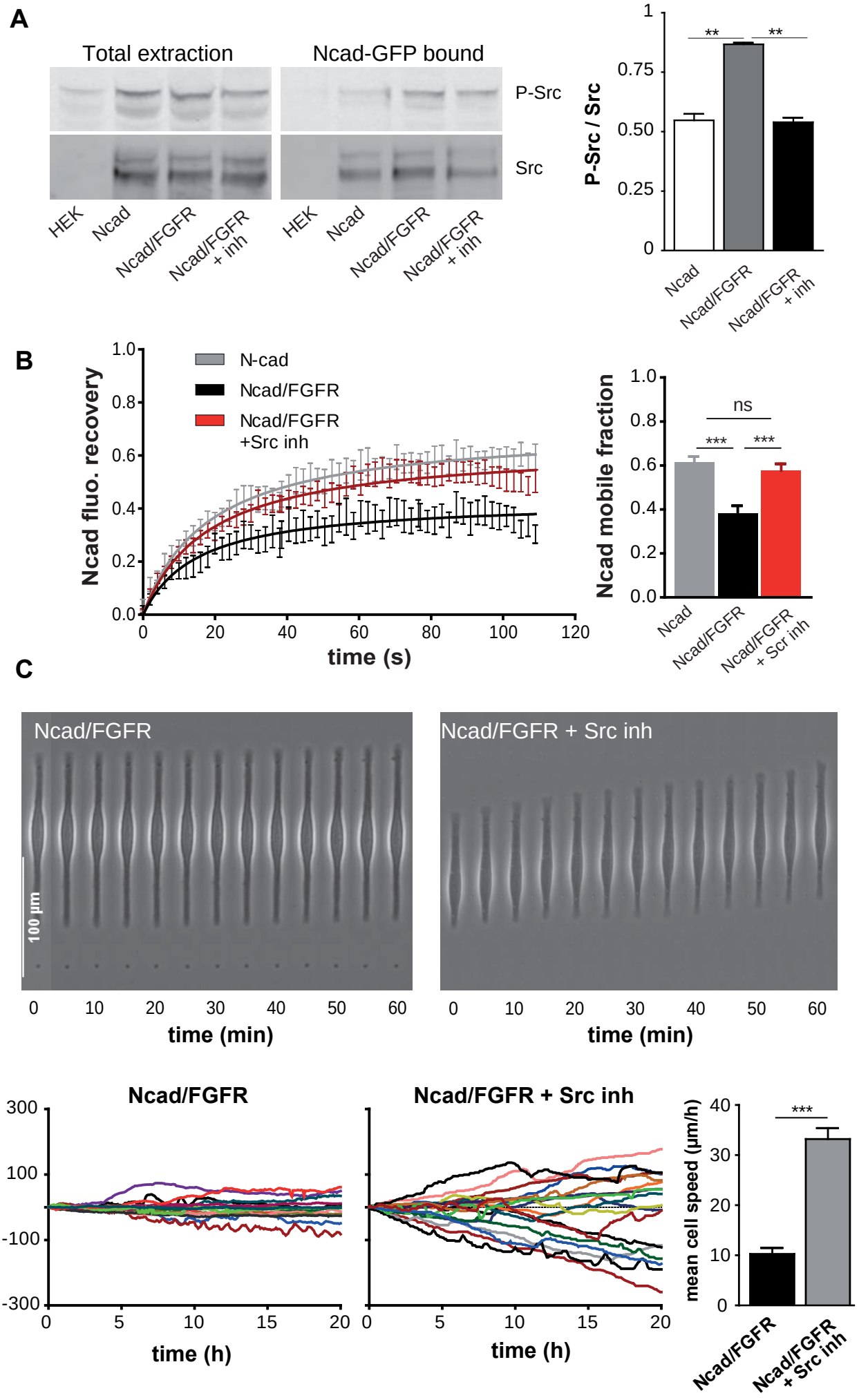

bioRxiv preprint doi: https://doi.org/10.1101/465930; this version posted November 8, 2018. The copyright holder for this preprint (which was not certified by peer review) is the author/funder. All rights reserved. No reuse allowed without permission.

Figure 9

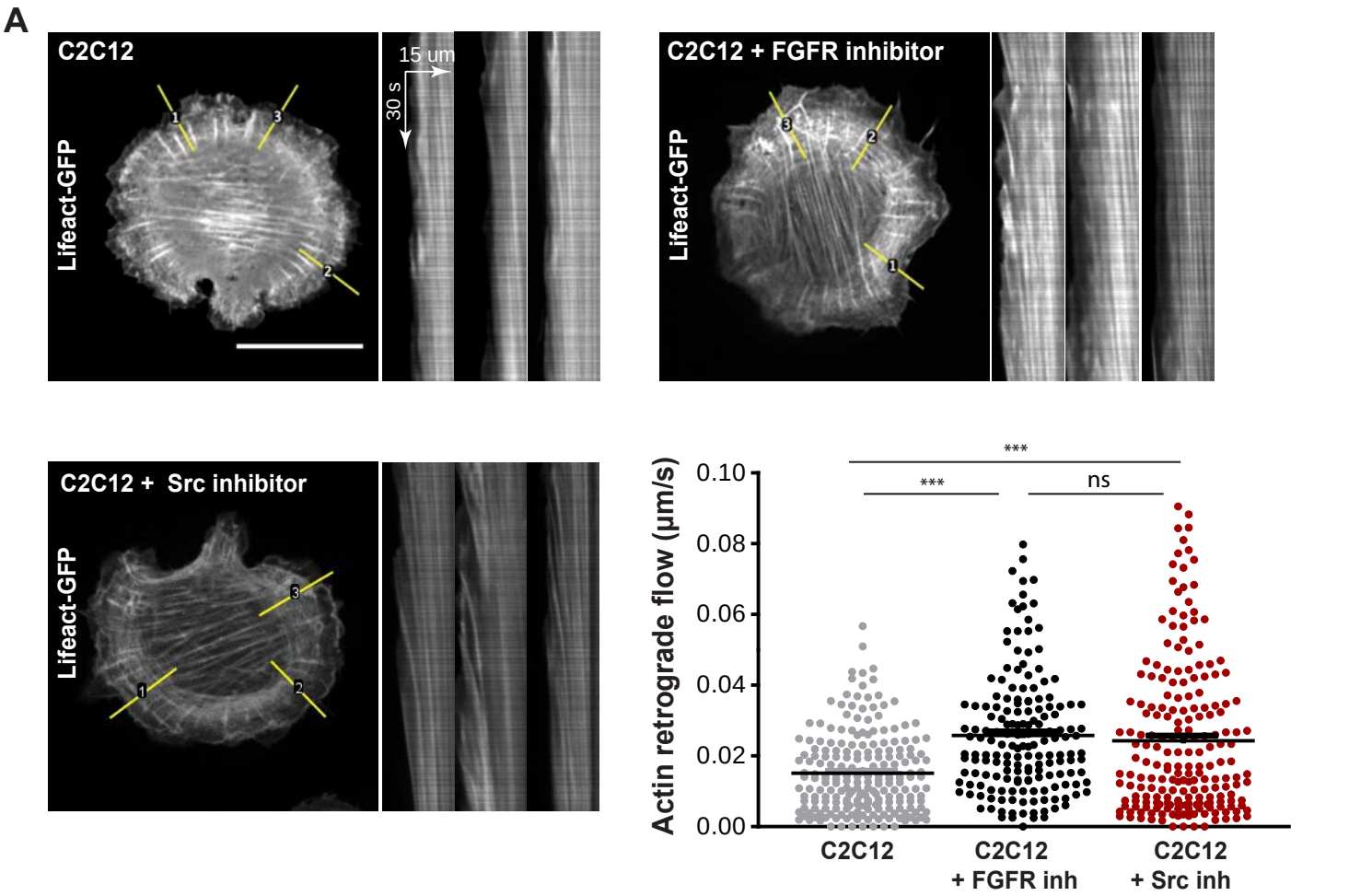

bioRxiv preprint doi: https://doi.org/10.1101/465930; this version posted November 8, 2018. The copyright holder for this preprint (which was not certified by peer review) is the author/funder. All rights reserved. No reuse allowed without permission.

Figure S1

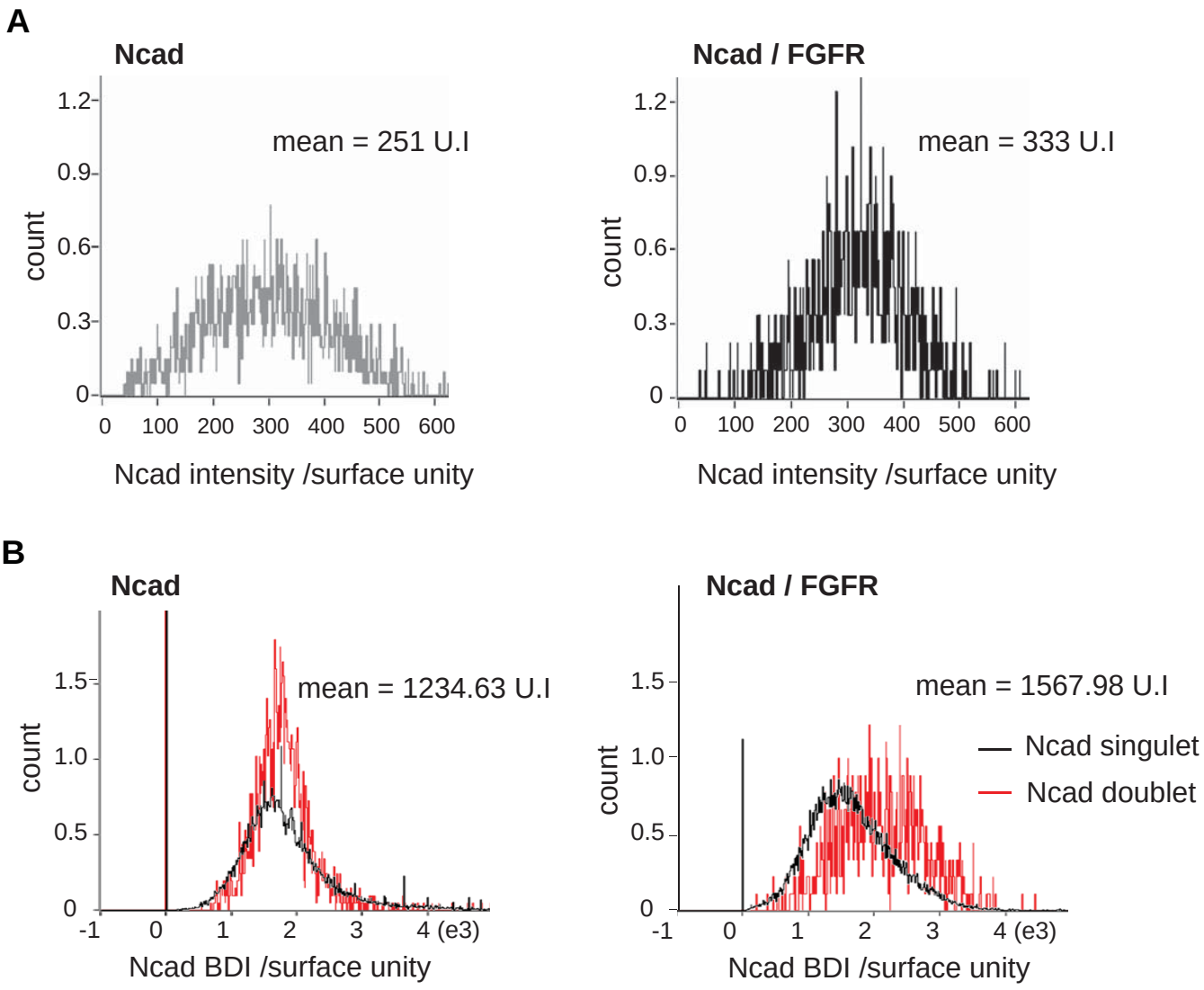

bioRxiv preprint doi: https://doi.org/10.1101/465930; this version posted November 8, 2018. The copyright holder for this preprint (which was not certified by peer review) is the author/funder. All rights reserved. No reuse allowed without permission.

Figure S2

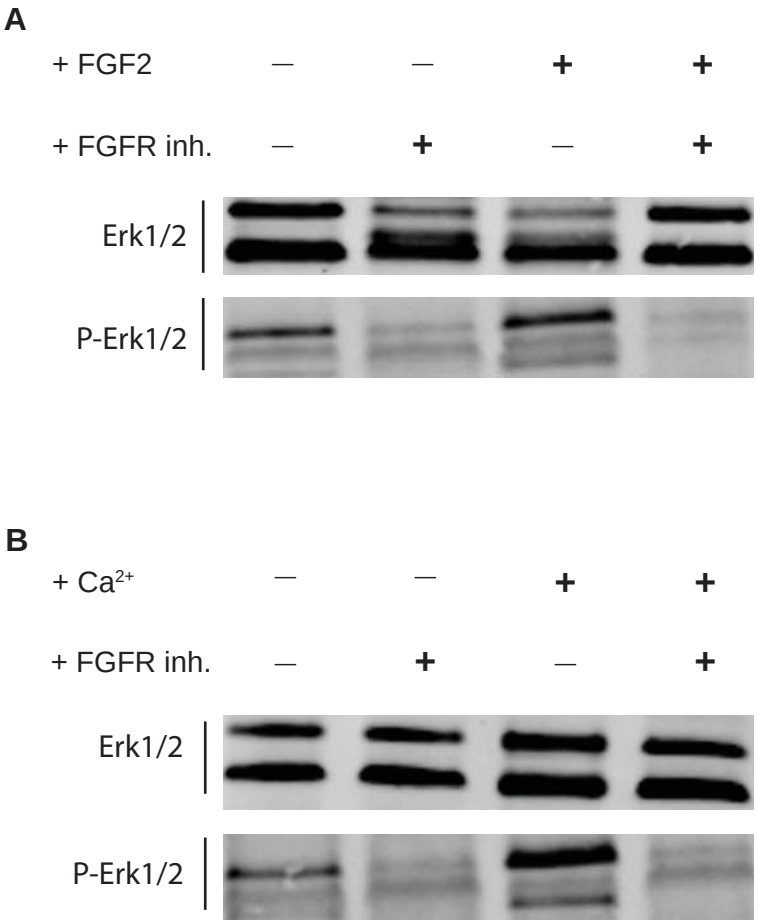

bioRxiv preprint doi: https://doi.org/10.1101/465930; this version posted November 8, 2018. The copyright holder for this preprint (which was not certified by peer review) is the author/funder. All rights reserved. No reuse allowed without permission.

Figure S3

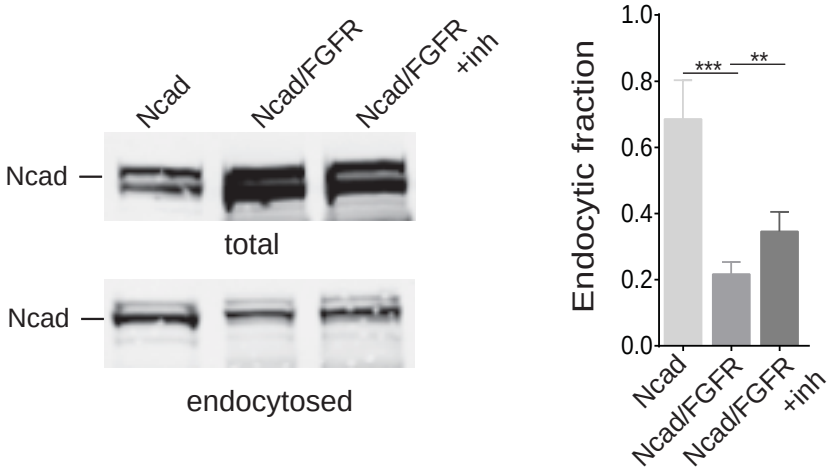

bioRxiv preprint doi: https://doi.org/10.1101/465930; this version posted November 8, 2018. The copyright holder for this preprint (which was not certified by peer review) is the author/funder. All rights reserved. No reuse allowed without permission.

Figure S4

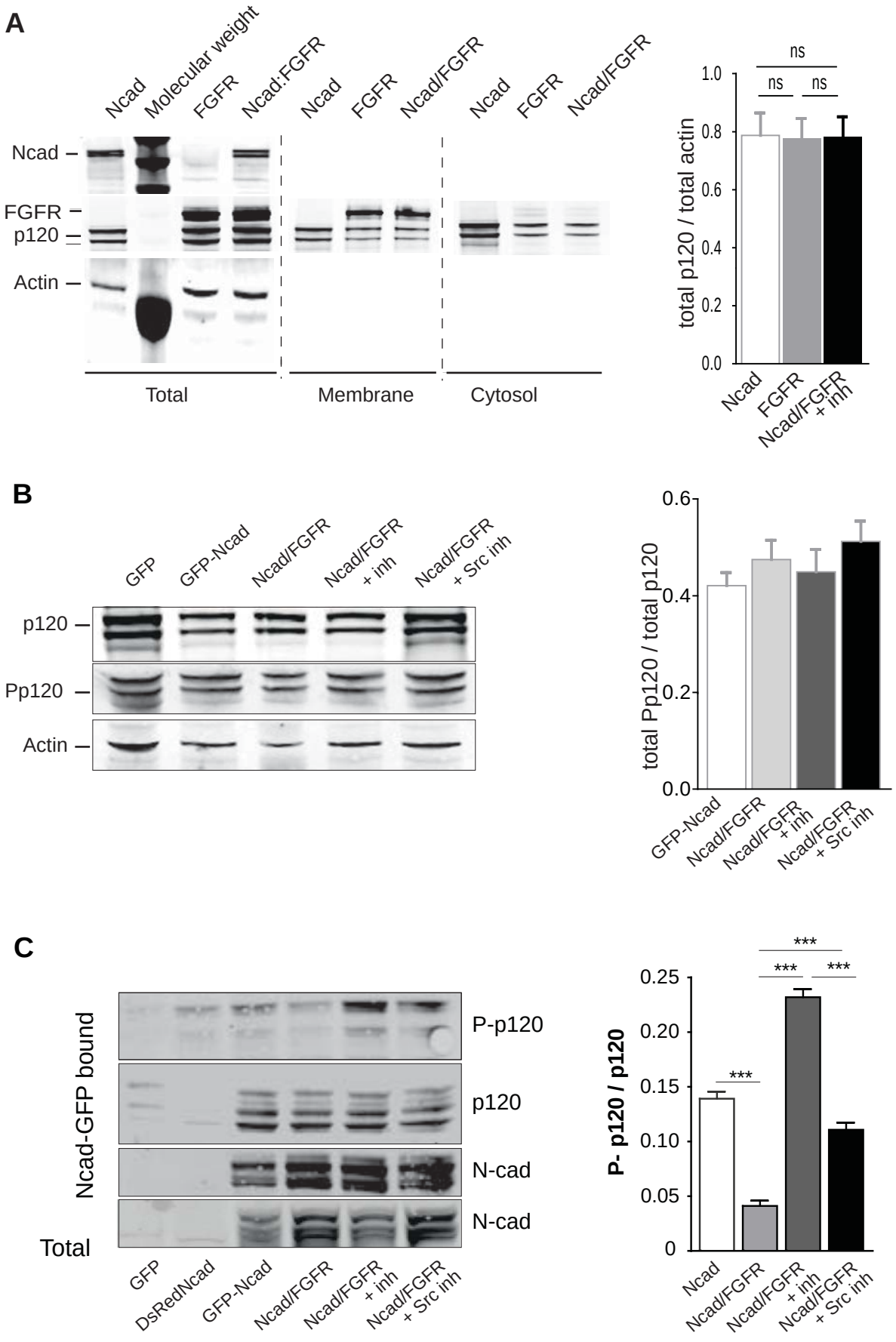

bioRxiv preprint doi: https://doi.org/10.1101/465930; this version posted November 8, 2018. The copyright holder for this preprint (which was not certified by peer review) is the author/funder. All rights reserved. No reuse allowed without permission.

Figure S5